Geochemistry Geophysics Geosystems G3

Article
Volume 13, Number 1
14 January 2012
Q01008, doi:10.1029/2011GC003845
ISSN: 1525-2027

Published by AGU and the Geochemical Society

Geochemical record of Holocene to Recent sedimentation on the Western Indus continental shelf, Arabian Sea

David R. Limmer
School of Geosciences, University of Aberdeen, Meston Building, Aberdeen AB24 3UE, UK (d.r.limmer@abdn.ac.uk)

Philipp Böning
ICBM Microbiogeochemistry, University of Oldenburg, D-26129 Oldenburg, Germany

Liviu Giosan and Camilo Ponton
Department of Geology and Geophysics, Woods Hole Oceanographic Institution, Woods Hole, Massachusetts 02543, USA

Cornelia M. Köhler
School of Geosciences, University of Aberdeen, Meston Building, Aberdeen AB24 3UE, UK

Matthew J. Cooper
School of Ocean and Earth Sciences, National Oceanography Centre, University of Southampton, Southampton SO14 3ZH, UK

Ali R. Tabrez
National Institute of Oceanography, ST-47 Block 1, Clifton, Karachi 75600, Pakistan

Peter D. Clift
School of Geosciences, University of Aberdeen, Meston Building, Aberdeen AB24 3UE, UK

[1] We present a multiproxy geochemical analysis of two cores recovered from the Indus Shelf spanning the Early Holocene to Recent (<14 ka). Indus-23 is located close to the modern Indus River, while Indus-10 is positioned ~100 km further west. The Holocene transgression at Indus-10 was over a surface that was strongly weathered during the last glacial sea level lowstand. Lower Holocene sediments at Indus-10 have higher ε_{Nd} values compared to those at the river mouth indicating some sediment supply from the Makran coast, either during the deposition or via reworking of older sediments outcropping on the shelf. Sediment transport from Makran occurred during transgressive intervals when sea level crossed the mid shelf. The sediment flux from non-Indus sources to Indus-10 peaked between 11 ka and 8 ka. A hiatus at Indus-23 from 8 ka until 1.3 ka indicates non-deposition or erosion of existing Indus Shelf sequences. Higher ε_{Nd} values seen on the shelf compared to the delta imply reworking of older delta sediments in building Holocene clinoforms. Chemical Index of Alteration (CIA), Mg/Al and Sr isotopes are all affected by erosion of detrital carbonate, which reduced through the Holocene. K/Al data suggest that silicate weathering peaked ca. 4–6 ka and was higher at Indus-10 compared to Indus-23. Fine-grained sediments that make up the shelf have geochemical signatures that are different from the coarser grained bulk sediments measured in the delta plain. The Indus Shelf data highlight the complexity of reconstructing records of continental erosion and provenance in marine settings.

Components: 12,300 words, 14 figures, 4 tables.

Keywords: Arabian Sea; Holocene paleoclimate; Indus; geochemistry; neodymium and strontium isotopes.

Index Terms: 0460 Biogeosciences: Marine systems (4800); 1039 Geochemistry: Alteration and weathering processes (3617); 1862 Hydrology: Sediment transport (4558).

Received 24 August 2011; **Revised** 7 November 2011; **Accepted** 6 December 2011; **Published** 14 January 2012.

Limmer, D. R., P. Böning, L. Giosan, C. Ponton, C. M. Köhler, M. J. Cooper, A. R. Tabrez, and P. D. Clift (2012), Geochemical record of Holocene to Recent sedimentation on the Western Indus continental shelf, Arabian Sea, *Geochem. Geophys. Geosyst.*, *13*, Q01008, doi:10.1029/2011GC003845.

1. Introduction

[2] Submarine fan systems potentially record the history of erosion in the world's largest continental drainage basins [*Kessarkar et al.*, 2005; *Bentahila et al.*, 2006; *Prytulak et al.*, 2006]. However, the deep-sea sediment record is separated from the surface processes at the source because of the finite transport time of sediment grains from source to sink. The Holocene global sea level rise of ca. 120 m has restricted sediment supply to many fan systems resulting in sediment storage within the shelf over the past 10 ka [*Vail et al.*, 1977; *Schattner et al.*, 2010]. Unless the shelf is narrow or sedimentation rates are exceptionally high, a record of continental erosion may only be preserved on the shelf, not on the abyssal plain, during periods of sea level rise [*Weber et al.*, 1997]. The shelf is thus potentially a crucial repository of erosional information spanning the Early Holocene because of high sedimentation rates near river mouths.

[3] In this study we attempt to understand the controls on sediment deposition in a major submarine delta and explore the factors controlling the movement and source of sediment using geochemical and visual analyses of cored sediments. We ask whether shelf sediments can be used to reconstruct the weathering and erosional impact of Holocene climate change on continental environments in SW Asia. To address this we have to know how clinoforms on the shelf have been built since the Holocene transgression. We focus on the Indus Shelf and sub-aqueous delta because this region receives a strong erosional flux and is subject to the influence of the Asian summer monsoon, which is known to have varied significantly since the Last Glacial Maximum (LGM) [*Fleitmann et al.*, 2003; *Gupta et al.*, 2003] (Figure 1).

[4] The weathering and erosional response to changing summer monsoon intensity in SW Asia is poorly constrained compared to river systems in SE Asia, where the summer monsoon is significantly stronger [*Colin et al.*, 2010; *Wan et al.*, 2010]. The Indus thus provides a chance to examine environmental change in a semi-arid river basin. In the Ganga Basin ε_{Nd} values and $^{87}Sr/^{86}Sr$ of river sediments are known to change on glacial time scales, changes that have been related to shifting Himalayan provenance and the large isotopic gradients known in the source regions [*Rahaman et al.*, 2009]. Sediments deposited at the Indus River mouth since 15 ka also show changes in Nd and Sr isotope character that have been interpreted to reflect a shift in erosion from the Karakoram to the Lesser Himalaya following the Last Glacial Maximum [*Clift et al.*, 2008a, 2010]. Curiously the direction of isotope change in the Indus delta (i.e., more negative ε_{Nd} values) implies more Lesser Himalayas erosion while that on the Ganga floodplain indicates the opposite (more positive ε_{Nd} values). On the Bengal Shelf the change is to more negative ε_{Nd} values, as seen in the Indus [*Tripathy et al.*, 2011]. Deeper water marine records in the Bay of Bengal have also been used to reconstruct changing provenance and chemical weathering intensity since the Last Glacial Maximum. *Colin et al.* [1999] used a combination of Nd and Sr isotopes together with clay mineralogy to argue for weaker chemical weathering in the Ganges-Brahmaputra catchment at the Last Glacial Maximum compared to the Holocene. They further argued that sediments in the Andaman Sea indicated that weathering intensity in the Irrawaddy River basin is mainly controlled by the summer monsoon rainfall intensity. In all these studies the effect of sediment reworking in shaping the sediment record is unknown.

[5] Over time periods $>10^5$ yr sediment supply to the Arabian Sea is expected to be controlled by changes in sea level, the westerly atmospheric system bringing moisture from Central Asia and Mediterranean [*Karim and Veizer*, 2002], as well as the monsoon intensity related to northern

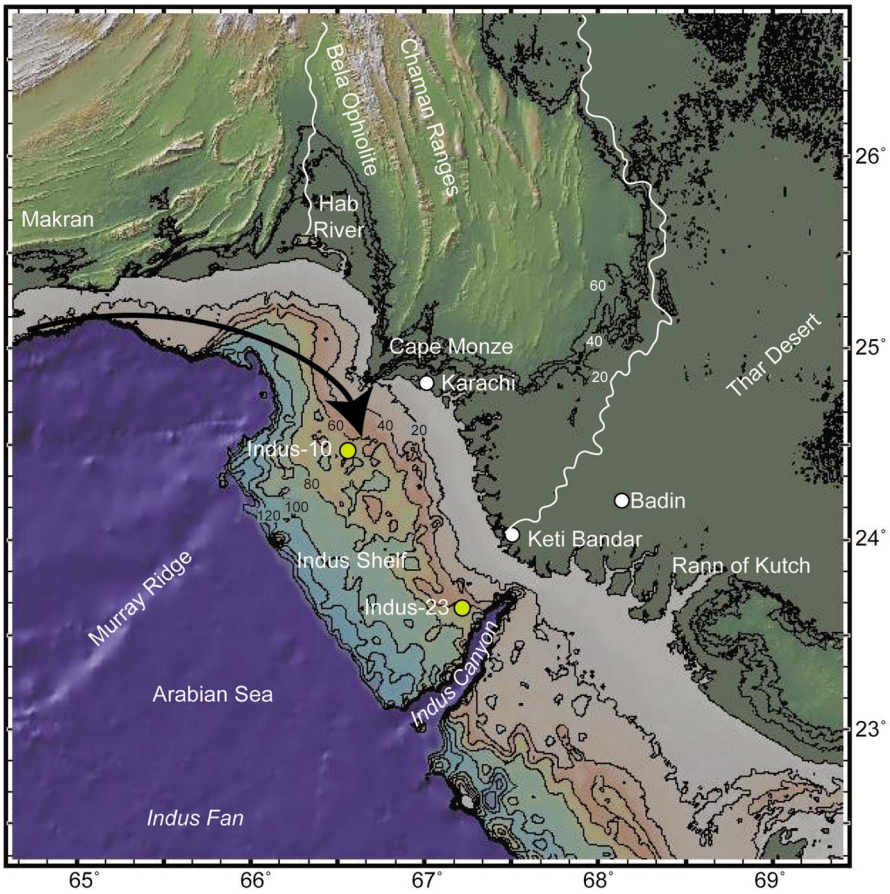

Figure 1. Bathymetric map showing core sites, locations of previous onshore work, the Indus River, Indus Fan and other features discussed in this text including the direction of the proposed longshore drift current. Bathymetry is from GeoMapApp and is contoured in 20 m intervals between 140 m depth and 60 m elevation above sealevel.

hemisphere climate. Both of these processes are thought to be controlled by orbitally modulated solar insolation [*Clemens et al.*, 1996; *Schulz et al.*, 1998]. Strong chemical weathering is generally associated with warmer, wetter conditions [*West et al.*, 2005], and might be expected to increase with intensifying monsoon [*Valdiya*, 1999]. However, increased precipitation may lead to a change in sediment residence times [*Dosseto et al.*, 2010; *Evrard et al.*, 2010], less rainfall could also increase sediment transport times allowing more weathering to occur. As a result the weathering response to monsoon climate change varies across Asia [*Clift et al.*, 2008b] and may also vary over different timescales because of the time required to transform pristine rock into a chemical weathered product.

[6] A study of clay minerals in the northeast floodplains of the Indus in Pakistan shows stronger chemical weathering linked to a weakening monsoon during the Late Holocene, yet at Keti Bandar close to the river mouth these same proxies argue for heightened chemical weathering at the time of a strong monsoon in the Early Holocene [*Alizai et al.*, 2012]. Here we examine how the marine delta record compares with the river mouth record sampled at Keti Bandar (Figure 1) by applying a variety of geochemical proxies to measure provenance and the varying chemical weathering intensity over the last deglacial cycle.

2. Geological Setting

[7] The Indus Shelf is a broad feature, forming the shallow water regions of the northern passive margin of the Arabian Sea (Figure 1). The shelf acts as a sink for sediment transported by the Indus River from the Karakoram and Western Himalayan regions [*Clift et al.*, 2002; *Garzanti et al.*, 2005]. The shelf stretches ca. 340 km from the Murray Ridge in the northwest to the Rann of Kutch to the southeast and runs ca. 120 km from the Indus Delta to the continental slope. The Indus Delta experiences

very high wave energies, and prior to human intervention received at least 250 × 10^6 t/yr from the Indus River [*Milliman et al.*, 1984; *Giosan et al.*, 2006]. This discharge is strongly seasonal, with the majority occurring between April and October, driven by glacial melting and the annual monsoon precipitation [*Karim and Veizer*, 2002].

[8] Radiocarbon dating indicates that sediment from the Indus River stopped feeding the submarine fan via the Indus Canyon at ca. 11 ka [*Prins et al.*, 2000], when sediment supply was outpaced by sea level rise [*Burgess and Hovius*, 1998]. However, coring close to the modern river mouth shows that sedimentation was rapid during the Holocene, with accumulations of >120 m recorded since 14 ka [*Clift et al.*, 2008a]. Offshore, some sediment reached the Indus Canyon, but this was not transported to the abyssal seafloor. The canyon is flanked by two major, asymmetric clinoforms [*Giosan et al.*, 2006] that reach onto the outer shelf on the eastern side of the canyon versus the mid shelf west of the canyon and appear to have been active in the recent past. In contrast, seismic surveys and coring of the outer shelf shows minimal to no Holocene sediment deposition at the shelf edge [*von Rad and Tahir*, 1997].

3. Materials

[9] In order to define the sources of the Holocene sediments on the Indus Shelf and assess their possible value as paleoclimatic archives, we present new Holocene records from two cores collected on the Western Indus Shelf. Cores were collected in December 2008 during cruise 64PE300 of the RV Pelagia. The cores for this study were selected close to the river mouth and canyon in the case of Indus-23 and in a more remote location, ca. 130 km northwest of the canyon in the case of Indus-10 (Figure 1). Both cores contain sediments younger than material cored on the upper fan by *Prins et al.* [2000]. Age control derived during this study reveals apparently continuous sedimentation after ca. 11 ka at Indus-10, but a major break in accumulation between 7.8 ka and 1.5 ka at Indus-23. Indus-10 represents a long duration record of sediment flux and changing environmental conditions since the Early Holocene, whereas Indus-23 provides the opportunity to explore the variability in geochemistry on centennial time scale in the Late Holocene.

4. Analytical Methods

[10] Major and trace element geochemistry, together with Nd and Sr isotopes, were employed as provenance and chemical weathering proxies because they have an established track record of being reliable in such settings [*Derry and France-Lanord*, 1996]. Certain elemental ratios were selected because they have been used in earlier studies as weathering proxies (e.g., Mg/Al, K/Al, K/Rb) or as proxies of silicate mass flux relative to carbonate (e.g., Ti/Ca). The chemical index of alteration (CIA) of *Nesbitt and Young* [1982] was also determine to estimate the intensity of weathering. Grain size analysis was also conducted for as many as samples as possible from both cores.

4.1. Age Model

[11] Age dating by ^{14}C methods was undertaken on mollusk shells at the National Ocean Sciences Accelerator Mass Spectrometry facility (NOSAMS, Woods Hole Oceanographic Institution) using their standard method discussed by *McNichol et al.* [1995]. Calibration of raw data to ages years BP was completed using the calibration data set Marine 04 of *Hughen et al.* [2009]. Table 1 shows the full list of material dated from both cores.

4.2. Major, Trace and Rare Earth Element Geochemistry

[12] For bulk elemental analysis all samples were freeze-dried and ground before mixing 600 mg of sample with 3600 mg of lithium tetraborate ($Li_2B_4O_7$, Spektromelt). The samples were pre-oxidized at 500°C with NH_4NO_3 and fused to glass-beads. Samples were then were analyzed for Si, Al, Ti, Fe, Na, Ca, K, P and Rb by X-Ray Fluorescence (XRF) using a Philips PW 2400 X-Ray spectrometer at the Institut für Chemie und Biologie des Meeres (ICBM) at the Carl von Ossietzky Universitaet, Oldenburg, Germany. XRF measurements were performed using the method of *Böning et al.* [2009]. Overall analytical precision and accuracy were monitored by measurements of several in-house standards and the certified standard GSD-3, and were better than 3%. All data were corrected for pore water salt contribution and are presented in Table 2.

4.3. Isotope Geochemistry

[13] Samples were digested in HCl, aqua regia, HNO_3, HF and $HClO_4$. A subsample equivalent to 1 μg of strontium and neodymium was taken. Neodymium was extracted through a two-stage process. Each sample was run through a cation extraction

Table 1. Calibrated Radiocarbon Ages for Shells Analyzed During This Study

Type	Sample	Depth (cm)	Age (yr BP)	Age Error (yr)	Calibrated Age 2 Sigma
Mollusc	Indus-10A-P-1,52 cm	826	10,050	45	10,815–11,177 yr BP
Mollusc	Indus-10A-P-2, 54 cm	728	5,650	40	6313–6526 yr BP
Mollusc	Indus-10A-P-4, 7 cm	479	3,020	15	2737–2842 yr BP
Mollusc	Indus-10A-P-3, 98 cm	674	4,980	20	5275–5432 yr BP
Mollusc	Indus-10A-P-2, 9 cm	683	4,980	20	5275–5432 yr BP
Mollusc	Indus-10A-P-4, 80 cm	554	4,000	20	3913–4089 yr BP
Mollusc	Indus-10A-P-5, 98 cm	472	3,020	15	2736–2842 yr BP
Mollusc	Indus-10A-P-7, 63 cm	291	2,850	15	2518–2704 yr BP
Mollusc	Indus-10A-P-9, 98 cm	128	1,180	25	662–780 yr BP
Mollusc	Indus-10A-P-10,12 cm	12	630	15	244–311 yr BP
Mollusc	Indus-23A-P-1, 80 cm	725	11,750	60	13,107 −13,318 yr BP
Mollusc	Indus-23A-P-1, 5 cm	650	7,310	40	7667–7873 yr BP
Mollusc	Indus-23A-P-2, 28 cm	580	1,910	35	1356–1544 yr BP
Mollusc	Indus-23A-P-6, 31 cm	220	765	30	315–475 yr BP
Mollusc	Indus-23A-P-7, 60 cm	149	695	25	279–415 yr BP

column to isolate the rare earth elements and then a Ln-Spec column extraction to isolate the Nd. Strontium was extracted using Sr-Spec resin columns apart from a few samples with high Ba where cation resin columns were used. Samples were loaded on the VG/Micromass Sector 54 thermo-ionization mass spectrometer (TIMS) at the National Oceanography Centre, Southampton (NOCS). Nd was mounted on the Ta sides of a triple Ta-Re-Ta filament assembly, Sr onto Ta single filaments with a Ta activator solution. The samples were both analyzed using multidynamic peak jumping routines. The longer term value for NBS987 was 0.710243 ± 0.000018 (2σ) on 93 and for JNdi 0.512092 ± 0.000014 (2σ) on 42. Neodymium isotope values were normalized to the chondrite uniform reservoir value and recorded as ε_{Nd} [*Goldstein et al.*, 1984]. The results are shown in Table 3.

4.4. Grain Size

[14] Grain size analysis was conducted using a Beckmann Coulter LS13 320 laser particle analyzer

Table 2. Major and Trace Element Geochemical Data for Sediments From Both Core Sites[a]

Sample	Rb	La	Ce	Pr	Nd	Sm	Eu	Gd	Tb	Dy	Ho	Er	Tm	Yb	Lu
Indus-10A-P-9, 91–93 cm	153	32.0	65.4	7.5	27.4	5.2	1.07	4.25	0.66	3.55	0.70	2.10	0.30	1.94	0.29
Indus-10A-P-7, 62–64 cm	121	31.9	65.0	7.6	28.0	5.4	1.09	4.43	0.67	3.56	0.68	2.05	0.29	1.84	0.27
Indus-10A-P-6, 34–36 cm	133	32.6	66.5	7.8	28.5	5.5	1.11	4.54	0.70	3.70	0.71	2.16	0.32	1.98	0.29
Indus-10A-P-4, 13–15 cm	126	27.4	55.9	6.5	23.7	4.5	0.92	3.62	0.57	2.92	0.56	1.73	0.25	1.55	0.23
Indus-10A-P-3, 34–35 cm	123	29.9	61.3	7.1	26.1	5.0	1.05	4.13	0.64	3.38	0.66	2.01	0.29	1.84	0.27
Indus-10A-P-2, 54–56 cm	117	29.6	60.8	6.9	25.5	4.9	1.01	4.05	0.63	3.33	0.66	2.01	0.28	1.78	0.27
Indus-10A-P-2, 73–75 cm	121	30.9	63.3	7.3	26.7	5.2	1.09	4.25	0.68	3.62	0.71	2.18	0.32	1.99	0.29
Indus-10A-P-2, 92–94 cm	123	28.7	58.8	6.8	24.9	4.8	1.01	3.90	0.62	3.32	0.65	2.02	0.30	1.85	0.28
Indus-10A-P-1, 11–13 cm	102	26.0	53.3	6.2	22.6	4.4	0.92	3.50	0.56	2.84	0.55	1.74	0.25	1.56	0.23
Indus-10A-P-1, 30–32 cm	91	23.5	48.6	5.6	20.6	3.9	0.85	3.20	0.51	2.59	0.49	1.60	0.23	1.41	0.21
Indus-10A-P-1, 49–51 cm	67	16.3	33.5	3.8	14.0	2.7	0.59	2.13	0.36	1.72	0.32	1.13	0.16	0.94	0.14
Indus-10A-P-1, 79–81 cm	163	33.8	69.1	7.9	28.9	5.5	1.12	4.48	0.71	3.81	0.75	2.27	0.34	2.13	0.32
Indus-23A-P-8, 86–88 cm	166	29.1	59.7	6.8	25.1	4.8	0.98	3.93	0.61	3.31	0.65	1.92	0.28	1.80	0.27
Indus-23A-P-7, 89–91 cm	164	32.2	66.0	7.6	27.6	5.2	1.08	4.35	0.66	3.50	0.68	2.05	0.30	1.85	0.27
Indus-23A-P-6, 13–15 cm	162	33.0	67.3	7.8	28.5	5.5	1.12	4.49	0.71	3.77	0.73	2.20	0.32	1.99	0.30
Indus-23A-P-5, 23–25 cm	158	27.4	56.0	6.5	23.6	4.6	0.94	3.74	0.60	3.09	0.61	1.87	0.27	1.65	0.25
Indus-23A-P-5, 81–83 cm	159	32.2	65.8	7.7	28.3	5.5	1.10	4.48	0.69	3.63	0.70	2.09	0.32	1.88	0.28
Indus-23A-P-4, 19–21 cm		33.6	68.9	7.8	28.7	5.5	1.13	4.53	0.71	3.83	0.76	2.23	0.33	2.09	0.31
Indus-23A-P-4, 89–91 cm	163	33.0	67.8	7.8	28.9	5.5	1.13	4.57	0.70	3.72	0.72	2.16	0.31	1.98	0.29
Indus-23A-P-3, 48–50 cm	153	25.9	52.9	6.2	22.8	4.4	0.89	3.56	0.57	2.99	0.58	1.81	0.26	1.61	0.23
Indus-23A-P-2, 4–6 cm	95	23.5	48.3	5.6	20.5	4.0	0.83	3.28	0.52	2.64	0.51	1.59	0.23	1.38	0.20
Indus-23A-P-2, 63–65 cm	171	29.6	60.4	7.0	25.4	4.9	0.98	3.89	0.62	3.26	0.63	1.95	0.29	1.79	0.26
Indus-23A-P-1, 22–24 cm	135	30.3	61.8	7.2	26.4	5.1	1.01	4.12	0.64	3.35	0.64	1.94	0.28	1.69	0.25
Indus-23A-P-1, 79–81 cm	135	30.6	62.1	7.2	26.2	5.1	1.01	4.10	0.63	3.26	0.62	1.88	0.27	1.66	0.24

[a]No XRF data was conducted on sample Indus-23A-P-4, 0 cm because of limited sample availability.

Table 3. Sr and Nd Isotope Data for Samples Taken From Cores Indus-10A-P and -23A-P, as Used in This Study

Sample	Depth (cm Below Seafloor)	$^{87}Sr/^{86}Sr$	±2 sigma	$^{144}Nd/^{143}Nd$	±2 sigma	εNd	Age (yr BP)
Indus-10A-P-9, 90 cm	120	0.715632	0.000013	0.512042	0.000006	−11.6	698
Indus-10A-P-7, 62 cm	290	0.713533	0.000014	0.512049	0.000006	−11.5	2,601
Indus-10A-P-6, 34 cm	362	0.714791	0.000023	0.512041	0.000007	−11.6	2,658
Indus-10A-P-4, 13 cm	487	0.712701	0.000010	0.512245	0.000010	-7.7	2,950
Indus-10A-P-3, 34 cm	608	0.712199	0.000011	0.512055	0.000015	-11.4	4,522
Indus-10A-P-2, 55 cm	729	0.711722	0.000013	0.512077	0.000016	-10.9	6,438
Indus-10A-P-2, 74 cm	748	0.711654	0.000021	0.512074	0.000033	-11.0	7,353
Indus-10A-P-2, 93 cm	767	0.711842	0.000010	0.512231	0.000011	-7.9	8,240
Indus-10A-P-1, 12 cm	786	0.710644	0.000013	0.512342	0.000011	-5.8	9,127
Indus-10A-P-1, 31 cm	804	0.710158	0.000016	0.512168	0.000009	-9.2	10,015
Indus-10A-P-1, 50 cm	824	0.709551	0.000011	0.512080	0.000007	-10.9	10,815
Indus-10A-P-1, 80 cm	854	0.718706	0.000013	0.51204	0.000008	-11.7	20000
Indus-23A-P-8, 87 cm	87	0.717456	0.000013	0.512033	0.000009	-11.8	169
Indus-23A-P-7, 90 cm	179	0.717671	0.000011	0.512013	0.000016	-12.2	367
Indus-23A-P-6, 14 cm	203	0.718778	0.000019	0.512015	0.000007	-12.2	383
Indus-23A-P-5, 24 cm	261	0.718853	0.000016	0.512006	0.000006	-12.3	510
Indus-23A-P-5, 82 cm	319	0.718994	0.000017	0.512120	0.000009	-10.1	673
Indus-23A-P-4, 20 cm	365	0.717918	0.000014	0.512054	0.000032	-11.4	803
Indus-23A-P-4, 90 cm	436	0.717671	0.000011	0.512055	0.000007	-11.4	999
Indus-23A-P-3, 48 cm	493	0.716440	0.000011	0.512013	0.000006	-12.2	1,163
Indus-23A-P-2, 5 cm	550	0.710184	0.000016	0.512019	0.000006	-12.1	1,323
Indus-23A-P-2, 64 cm	609	0.717378	0.000020	0.512201	0.000018	-8.5	1,489
Indus-23A-P-1, 22 cm	667	0.712577	0.000010	0.512066	0.000019	-11.2	8,868
Indus-23A-P-1, 80 cm	725	0.713670	0.000016	0.511987	0.000006	-12.7	13,107

at the University of Aberdeen. A small fraction of sample was placed in a 25 ml beaker. Five ml of distilled water and two to three drops of Calgon solution. Samples were stirred with a glass stirrer and left in a sonic bath for 10 min. The material was then poured into a sampling tube before being placed on the turntable of the laser particle analyzer. The samples were then sonicated for a further 30 seconds by the built-in sonic probe before being run. Each sample was run three times. The analysis yields average grain size and these are shown in Table 4.

5. Results

5.1. Sedimentation History

[15] Both Sites Indus-10 and -23 are located at ca. 70 m water depth (Figure 1). Both cores are principally composed of clay-rich, muddy material with occasional layers or lenses of silt, with variable frequency, often forming fining-up sequences typically less than 10 cm thick, but ranging up to 20 and even 50 cm thick at the base of Indus-10 (Figures 2c, 2d, 2e, 3 and 4). Whole and fragmented gastropod and bivalve shells are found sparsely in the core. Both cores display gray-black laminations within the clay-rich layers (Figures 2b and 2f).

[16] Sediment at ca. 800 cm and 730 cm below seafloor respectively was dated by radiocarbon methods at 11.1 ka and 13.1 ka at Indus-10 and Indus-23 respectively. Sedimentation at Indus-10 is continuous after 11.1 ka above a clear iron-stained unconformity (Figures 2a and 3) located at ca. 830 cm depth at Indus-10, where a 50-cm-thick fining upwards sand layer is observed overlying a burrowed, more consolidated, orange-stained clay (Figure 2a). A condensed interval with sedimentation rates of ca. 20 cm/k.y. occurs from the Early Holocene until ca. 6.4 ka; sedimentation rates increase after that to between 60 and 190 cm/k.y. A major break in preservation is also inferred at Indus-23 where most of the Middle Holocene is missing (Figures 2d and 4). Even below this interval sedimentation is highly condensed in the Lower Holocene, averaging 17 cm/k.y. compared to 1014 cm/k.y. at the top of the core.

5.2. Major Elemental Geochemistry

[17] Figures 3 and 4 display lithological, isotopic and selected elemental geochemistry for Indus-10 and Indus-23 plotted against core depth. The two cores have different major and trace elemental compositions. Mg/Al is very low below the unconformity and then rises sharply just above this level at Indus-10 before falling back to lower

Table 4. Grain Size Data for Indus-10 and Indus-23

File Name	Age (yr BP)	Depth (cmbsf)	Average Grain Size (μm)	Standard Deviation	Median	Average Mode (μm)	Average Skewness	Average Kurtosis
10AP-10, 0 cm	0	0	20.45	35.9	7.31	6.45	2.92	9.62
10AP-10, 20 cm	357	20	20.35	35.7	7.28	13.12	2.95	9.84
10AP-9, 0 cm	437	28	20.44	35.8	7.31	13.67	2.93	9.58
10AP-9, 20 cm	635	48	20.77	36.4	7.34	13.67	2.89	9.06
10AP-9, 28 cm	715	56	14.78	32.6	3.86	4.88	3.47	11.65
10AP-9, 40 cm	716	68	21.11	37.0	7.36	13.69	2.84	8.75
10AP-9, 50 cm	717	78	21.31	37.6	7.37	13.72	2.87	8.88
10AP-9, 60 cm	718	88	20.96	36.8	7.33	12.69	2.85	8.79
10AP-9, 80 cm	719	108	21.34	36.9	7.76	13.20	2.83	8.63
10AP-8, 0 cm	721	128	21.61	36.9	8.00	14.54	2.81	8.68
10AP-8, 20 cm	802	148	21.58	36.7	8.05	14.68	2.82	8.77
10AP-8, 40 cm	884	168	21.49	36.5	8.14	12.02	2.83	8.89
10AP-8, 60 cm	1139	188	21.51	36.5	8.21	12.09	2.84	8.89
10AP-8, 64 cm	1196	192	21.43	36.5	8.12	45.75	2.85	8.93
10AP-8, 80 cm	1425	208	16.58	34.8	4.35	5.88	3.46	12.30
10AP-8, 96 cm	1653	224	20.19	38.0	6.03	7.54	3.02	8.94
10AP-7, 0 cm	1711	228	25.79	45.7	6.02	8.54	2.24	3.94
10AP-7, 20 cm	1996	248	19.63	41.9	3.98	5.35	2.98	6.55
10AP-7, 31 cm	2154	259	24.33	46.7	5.00	6.45	2.47	5.05
10AP-7, 40 cm	2282	268	20.93	41.8	4.71	5.88	2.78	7.00
10AP-7, 50 cm	2425	278	18.11	38.5	4.17	5.35	3.20	9.88
10AP-7, 60 cm	2568	288	15.96	33.4	4.73	6.45	3.60	13.33
10AP-7, 80 cm	2628	308	15.33	36.8	3.39	4.73	3.50	11.73
10AP-6, 0 cm	2647	328	17.54	37.1	3.49	9.37	3.03	8.51
10AP-6, 20 cm	2667	348	13.32	29.3	3.95	5.88	4.04	17.40
10AP-6, 40 cm	2687	368	16.89	33.7	5.81	8.54	3.62	13.60
10AP-5, 0 cm	2693	374	21.84	39.4	7.16	9.32	2.93	8.43
10AP-5, 20 cm	2712	394	24.08	41.2	7.44	9.37	2.56	6.01
10AP-5, 40 cm	2732	414	24.75	44.2	8.48	12.40	2.74	6.91
10AP-5, 50 cm	2742	424	20.61	39.7	4.72	5.35	2.84	7.79
10AP-5, 60 cm	2752	434	19.21	34.0	7.36	10.29	3.23	10.82
10AP-5, 80 cm	2771	454	25.77	46.1	6.70	8.54	2.45	5.09
10AP-4, 0 cm	3102	474	20.11	39.0	5.46	7.53	3.07	9.40
10AP-4, 20 cm	3327	494	20.40	39.4	5.51	7.59	3.01	8.99
10AP-4, 40 cm	3552	514	20.63	39.8	5.52	7.62	2.97	8.60
10AP-4, 60 cm	3776	534	19.47	36.2	5.66	9.89	2.91	9.20
10AP-4, 80 cm	4001	554	19.85	36.8	5.72	10.03	2.79	7.95
10AP-3, 0 cm	4226	574	20.29	37.9	5.73	8.36	2.85	8.23
10AP-3, 20 cm	4450	594	21.88	37.9	7.90	9.37	2.90	8.29
10AP-3, 40 cm	4563	604	19.67	37.0	5.69	7.91	2.90	8.52
10AP-3, 60 cm	4787	624	13.58	14.4	8.35	6.45	1.36	1.23
10AP-3, 70 cm	4900	634	30.13	49.4	9.35	5.88	2.27	4.35
10AP-3, 80 cm	5012	644	21.65	36.7	8.10	14.82	2.81	8.72
10AP-2, 0 cm	5349	674	21.75	36.9	8.09	5.88	2.79	8.60
10AP-2, 20 cm	5611	694	21.52	36.5	8.14	9.37	2.82	8.83
10AP-2, 40 cm	6086	714	21.45	36.4	8.16	12.40	2.84	8.93
10AP-2, 50 cm	6324	724	21.51	36.5	8.19	11.29	2.83	8.87
10AP-2, 60 cm	6694	734	20.60	36.4	7.11	7.08	2.89	9.14
10AP-2, 80 cm	7611	754	20.54	36.4	7.08	10.94	2.90	9.16
10AP-1, 0 cm	8528	774	20.36	35.7	7.29	13.62	2.96	10.05
10AP-1, 10 cm	8986	784	20.71	36.3	7.34	6.45	2.90	9.15
10AP-1, 20 cm	9445	794	20.84	36.6	7.33	13.62	2.86	8.85
10AP-1, 40 cm	9903	804	21.11	37.0	7.36	13.69	2.84	8.75
10AP-1, 60 cm	10820	824	21.37	37.6	7.38	13.73	2.86	8.84
10AP-1, 80 cm	>20,000	844	21.01	37.0	7.34	12.68	2.87	8.90
10AP-1, 90 cm	>20,000	854	21.30	37.0	7.65	13.10	2.82	8.56
10AP-CC, 0 cm	>20,000	874	20.45	36.0	7.30	13.05	2.92	9.61
10AP-CC, 20 cm	>20,000	894	20.37	35.8	7.31	8.54	2.94	9.78
23AP-8, 0 cm	0	0	27.87	40.49	14.36	18.03	2.53	4.73
23AP-8, 7 cm	16	7	31.24	45.70	13.77	28.70	2.16	4.20
23AP-8, 20 cm	47	20	46.96	58.85	15.93	18.00	1.47	1.51

Table 4. (continued)

File Name	Age (yr BP)	Depth (cmbsf)	Average Grain Size (μm)	Standard Deviation	Median	Average Mode (μm)	Average Skewness	Average Kurtosis
23AP-8, 40 cm	93	40	24.53	42.13	8.68	7.78	2.77	6.87
23AP-8, 60 cm	140	60	18.66	33.19	6.79	10.65	3.20	10.99
23AP-8, 74 cm	172	74	27.93	45.14	9.06	59.53	2.35	4.88
23AP-8, 80 cm	186	80	13.63	20.85	7.02	10.23	2.22	5.62
23AP-7, 0 cm	207	89	28.92	52.08	3.91	11.29	2.47	7.13
23AP-7, 20 cm	254	109	25.64	45.62	8.32	9.89	2.58	5.84
23AP-7, 30 cm	277	119	13.66	25.05	5.84	9.37	5.78	48.14
23AP-7, 40 cm	300	129	22.93	38.17	9.33	13.61	2.82	7.84
23AP-7, 60 cm	347	149	18.25	37.33	5.83	7.78	3.43	11.86
23AP-7, 70 cm	354	159	28.28	49.39	7.60	12.40	2.30	4.42
23AP-7, 80 cm	361	169	21.75	36.41	8.71	12.06	3.13	10.96
23AP-6, 0 cm	374	189	28.62	45.10	8.34	8.15	2.19	4.19
23AP-6, 20 cm	388	209	39.94	62.63	9.31	139.10	1.94	2.80
23AP-6, 30 cm	394	219	23.14	41.29	7.57	10.29	2.84	8.83
23AP-6, 40 cm	472	229	23.71	41.39	8.25	12.40	2.95	8.85
23AP-5, 0 cm	540	237	20.59	36.11	7.37	9.37	2.89	8.30
23AP-5, 20 cm	711	257	21.17	34.63	8.78	9.37	3.04	10.08
23AP-5, 32 cm	814	269	19.60	28.14	9.80	11.29	2.24	5.48
23AP-5, 40 cm	869	277	33.68	42.50	16.99	5.88	2.24	5.88
23AP-5, 60 cm	908	297	19.04	33.58	6.94	10.29	3.12	10.27
23AP-5, 80 cm	947	317	29.57	44.34	12.94	27.59	2.53	6.52
23AP-4, 0 cm	1002	345	21.14	35.59	8.42	10.96	3.07	10.04
23AP-4, 20 cm	1042	365	8.69	9.62	5.69	8.54	1.74	2.98
23AP-4, 40 cm	1081	385	15.02	29.97	5.39	8.54	3.77	15.13
23AP-4, 50 cm	1101	395	16.87	37.30	4.20	5.88	3.26	10.03
23AP-4, 60 cm	1120	405	15.28	32.95	5.32	7.78	3.92	15.68
23AP-4, 80 cm	1159	425	19.52	38.14	6.07	8.54	3.07	8.93
23AP-3, 0 cm	1199	445	19.77	36.13	7.11	9.37	3.13	9.87
23AP-3, 20 cm	1238	465	19.70	34.45	7.51	9.37	3.34	12.37
23AP-3, 30 cm	1258	475	17.08	31.49	5.56	9.37	3.25	11.40
23AP-3, 40 cm	1277	485	19.20	33.36	7.10	8.83	3.18	11.09
23AP-3, 60 cm	1317	505	23.06	39.72	8.80	13.65	3.01	9.36
23AP-3, 70 cm	1336	515	32.38	45.96	13.95	15.91	2.17	4.35
23AP-3, 80 cm	1356	525	26.24	44.48	8.30	9.98	2.53	5.93
23AP-3, 98 cm	1391	543	28.39	44.39	11.06	18.39	2.43	5.44
23AP-2, 0 cm	1395	545	18.51	33.13	7.22	11.11	4.47	29.86
23AP-2, 20 cm	1434	565	14.63	20.56	7.74	10.96	1.81	3.39
23AP-2, 40 cm	1474	585	15.48	29.20	6.47	9.37	4.08	18.89
23AP-2, 60 cm	1513	605	23.66	45.88	5.51	7.31	2.51	5.25
23AP-2, 70 cm	1532	615	23.56	40.93	8.13	11.29	2.73	7.03
23AP-2, 80 cm	5797	625	27.83	40.13	11.13	11.43	2.29	6.14
23AP-2, 98 cm	7302	643	29.44	51.99	6.71	203.50	2.44	5.24
23AP-1, 0 cm	7469	645	35.79	50.02	12.39	168.90	2.10	4.33
23AP-1, 20 cm	8955	665	21.14	37.69	8.83	13.21	3.68	15.48
23AP-1, 40 cm	10379	685	29.47	35.69	19.03	24.76	2.44	6.71
23AP-1, 60 cm	11803	705	32.31	36.71	21.15	23.27	2.25	5.36
23AP-1, 80 cm	13227	725	26.24	34.08	13.40	12.40	1.91	3.43
23AP-1, 90 cm	13300	735	35.62	48.72	4.68	61.48	2.47	5.41
23AP-1, 98 cm	13450	743	23.69	39.79	7.92	11.29	2.79	8.27
23AP-CC, 0 cm	13600	745	23.12	38.05	6.68	7.36	2.78	8.96
23AP-CC, 20 cm	13650	765	18.86	39.89	4.95	9.37	3.16	9.52

values. The CIA behaves in a similar fashion, being very high under the unconformity and then rising sharply above that hiatus. K/Al behaves in a different fashion because this is very high under the unconformity and then falls to progressively lower values above that level.

[18] Contrasting trends are seen at Indus-23. Mg/Al and K/Al are higher at the base of the core below 600 cm below seafloor (cmbsf), above which the sedimentation rates rise sharply. Mg/Al and K/Al both fall to a more constant lower value above that level (Figure 4). CIA is high immediately below

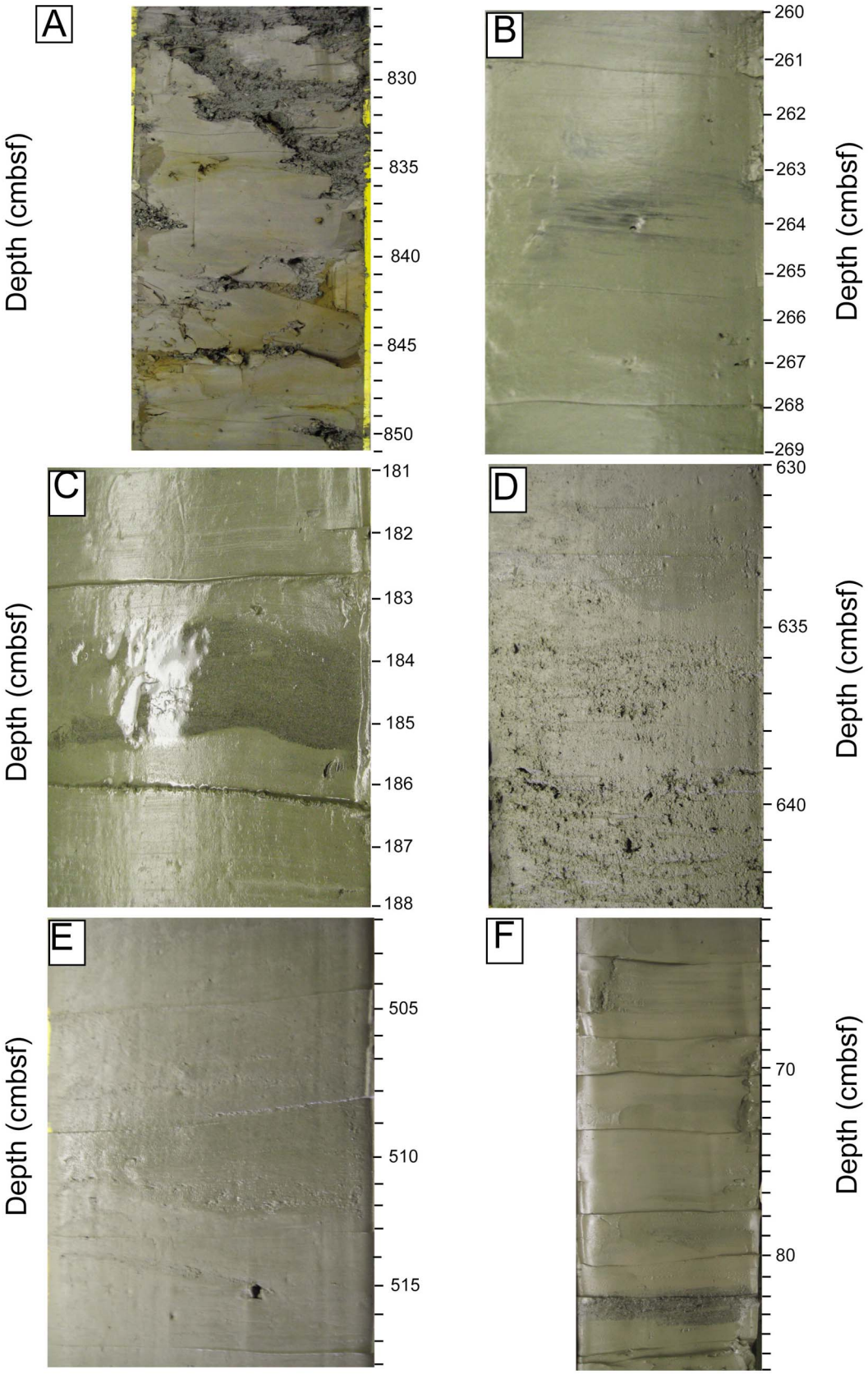
A
Depth (cmbsf)
830
835
840
845
850
B
260
261
262
263
264
265
266
267
268
269
Depth (cmbsf)
C
Depth (cmbsf)
181
182
183
184
185
186
187
188
D
630
635
640
Depth (cmbsf)
E
Depth (cmbsf)
505
510
515
F
70
80
Depth (cmbsf)

Figure 2

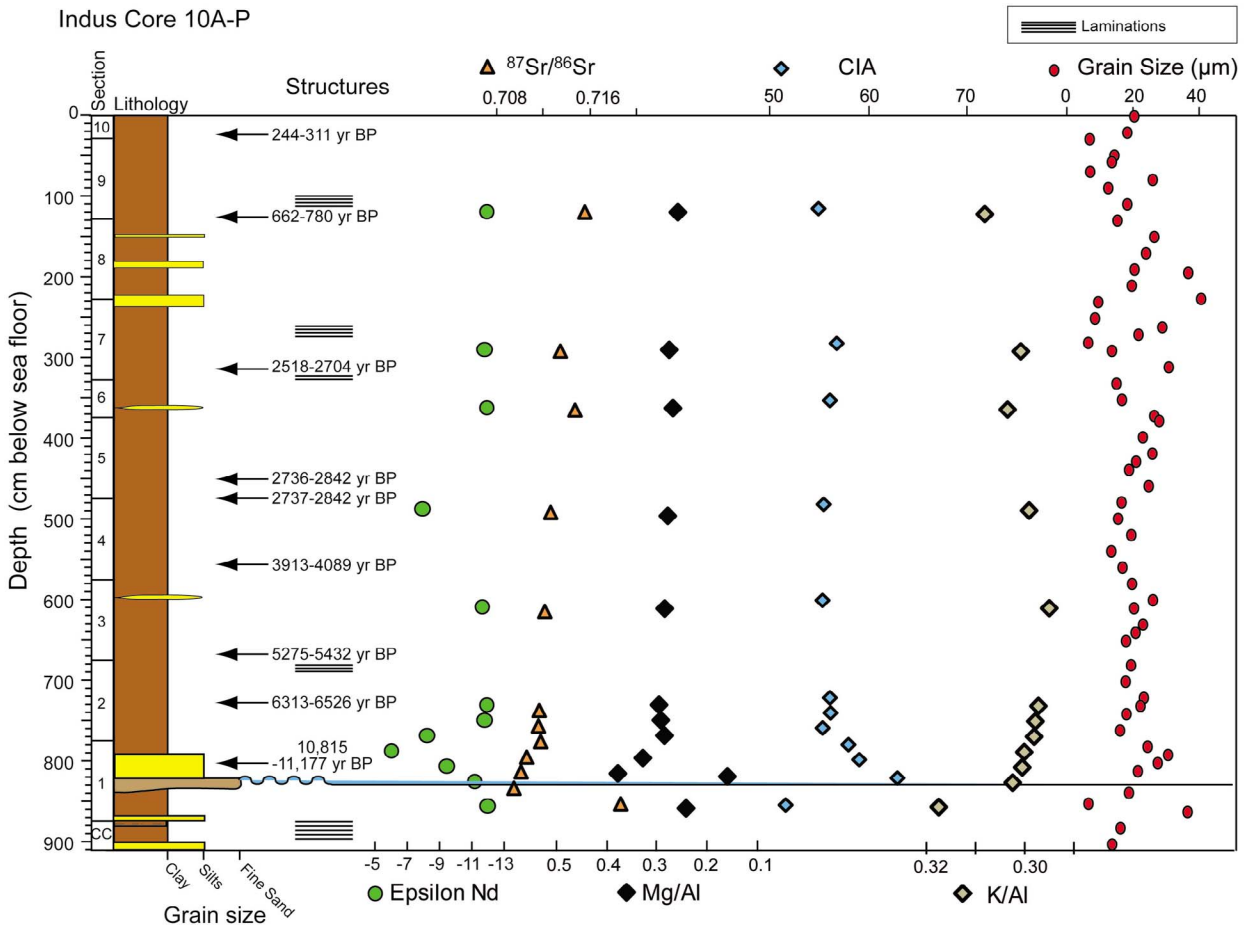

Figure 3. Sedimentary log for Site Indus-10, showing grain size, isotope and geochemical variations. Note two major shifts in ε_{Nd} values and a net increase in $^{87}Sr/^{86}Sr$ above the Last Glacial unconformity. The ε_{Nd} value beneath the unconformity is not significantly different from sediment above this surface, but the $^{87}Sr/^{86}Sr$ value is much higher.

600 cm, but falls to lower values deeper in the core. One exceptional sample was found at 550 cmbsf showing very low CIA, K/Al and high Mg/Al.

5.3. Rare Earth Elements

[19] Rare earth element (REE) geochemistry is best considered by normalizing concentrations to C1 Chondrite for all samples [*Anders and Grevesse*, 1989]. The patterns for both Indus-10 and Indus-23 samples are fairly typical of continental crustal material in being light REE-enriched. The samples show a particular enrichment in the LREEs, while the heavy REEs display a flatter pattern (Figures 5a and 5b). All samples show a well-developed negative Eu anomaly, which is typical of rocks eroded from sources that have experienced plagioclase fractionation, such as granites. At Indus-10 samples from just above the unconformity have lower REE concentrations than the upper part of the core, which shows comparable values to those found at Indus-23.

[20] REE values were also normalized against the upper continental crust values of *Rudnick and Fountain* [1995] (Figures 5c and 5d). Once again greater variability is observed at Indus-10, where samples located just above the unconformity show

Figure 2. Photographs of core material from Indus-10 and -23, showing (a) the unconformity near the base of Indus-10, a transition from red-orange clays to black shell-rich sands, (b) black, organic sulphide rich laminations from the middle of Indus-10A-P-7 (ca. 260 cm below seafloor), (c) fining upward sandy horizon from the middle of Indus-10A-P-8 (190 cm below seafloor), (d) silty, fining upwards section at the bottom of Indus-23A-P-2, a possible unconformity (643 cm below seafloor), (e) silt-fine sand horizon from the middle of Indus-23AP-3 (505 cm below seafloor), and (f) black, slightly silty laminations from bottom half of Indus-23AP-8 (80 cm below seafloor).

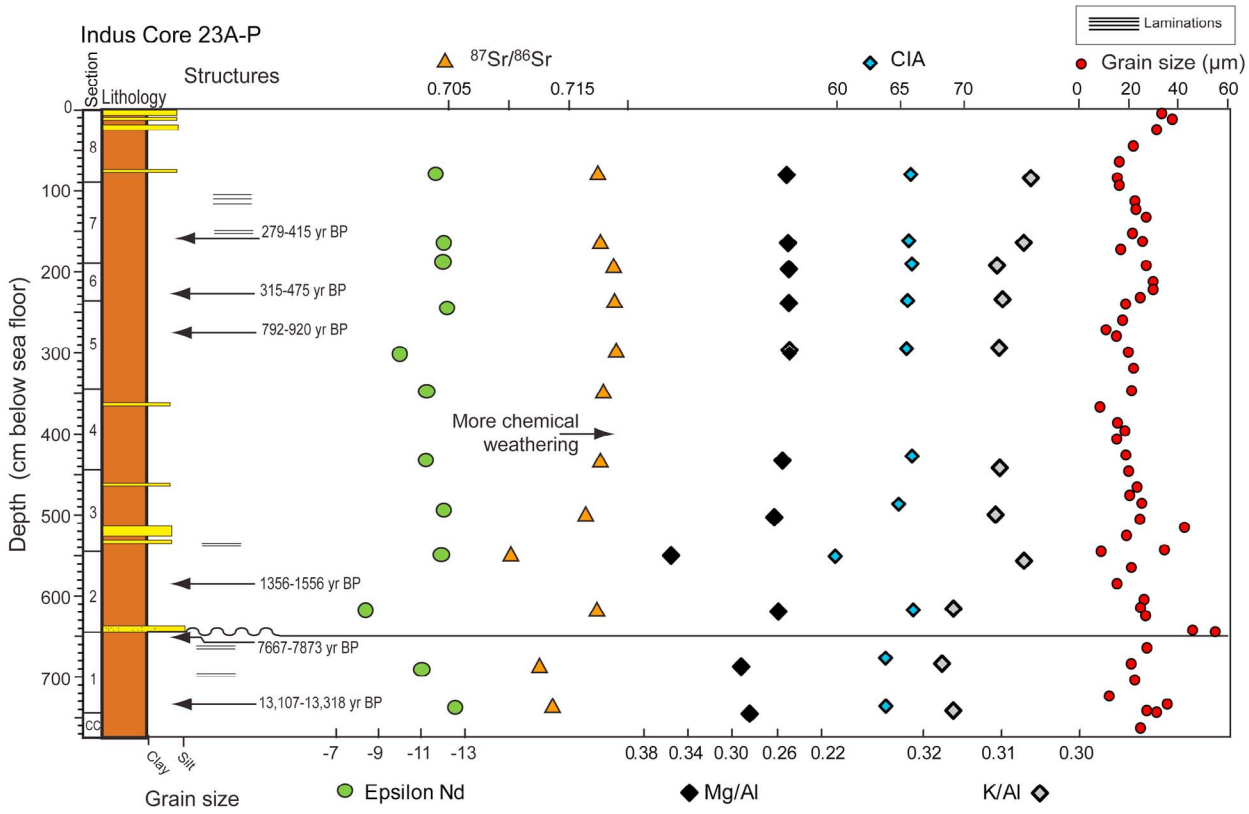

Figure 4. Sedimentary log for Site Indus-23, showing grain size, isotope and elemental geochemical variations close to the modern canyon, and in particular a possible unconformity and two moderate rise in ε_{Nd} values at 609 cm and 319 cm below seafloor, together with significant variation in $^{87}Sr/^{86}Sr$ values. Shifts in ε_{Nd} value are smaller than in Indus-10A-P, while $^{87}Sr/^{86}Sr$ values are consistently higher.

more depletion in all elements relative to upper continental crust compared to the younger samples and those below the unconformity. In general the sediments at both sites are close to or mildly depleted in REEs compared to bulk upper continental crust. Sediments from both Indus-10 and -23 show relative depletion in the HREEs and a mild depletion in the LREEs, with the highest relative values in Sm, Eu, Gd and Tb.

5.4. Isotopic Variations

[21] The Nd and Sr isotope characteristics of the sediments in each core can be compared, recognizing that Indus-23 largely represents sedimentation spanning only the last 1600 years, while Indus-10 provides the longer-term record since ca. 11 ka. Indus-10 generally shows ε_{Nd} values of ca. −12, except for one interval near the base centered at 786 cm and another sample at 487 cm depth where higher ε_{Nd} values are encountered (Figure 3). ε_{Nd} rises at 786 cm to a value of −5.8, correlating with an increase in $^{87}Sr/^{86}Sr$ and CIA, but a decrease in Mg/Al, Ti/Al, and K/Al. The rise in ε_{Nd} in the sample at 487 cm is smaller, reaching only −7.7, but this is not matched by significant changes in $^{87}Sr/^{86}Sr$ values and K/Al, which are gradually increasing at this time, while Mg/Al, and CIA are roughly stable. $^{87}Sr/^{86}Sr$ values increase up-core in Indus-10, especially between 830 and 750 cm below seafloor. The highest $^{87}Sr/^{86}Sr$ value is recorded below the unconformity, where it reaches 0.7187.

[22] Sediments from Indus-23 (Figure 4) also show two rises in ε_{Nd} values. A rise to an ε_{Nd} value of −8.5 occurs at 617 cm depth in a part of the core where $^{87}Sr/^{86}Sr$ is at a maximum, CIA values increase, and Mg/Al, K/Al and K/Rb all decrease. This interval lies just below an unconformity or hiatus in sedimentation. The precise level of the break or dramatic slowing in sedimentation is unclear and is only bracketed as being between 580 and 650 cmbsf by the ^{14}C dating. A smaller rise in ε_{Nd} values from −13 to −10.1 is seen at a depth of 319 cm, where $^{87}Sr/^{86}Sr$ values are rising, Mg/Al decreases, and K/Al and CIA remain approximately constant. The highest $^{87}Sr/^{86}Sr$ values of 0.7189

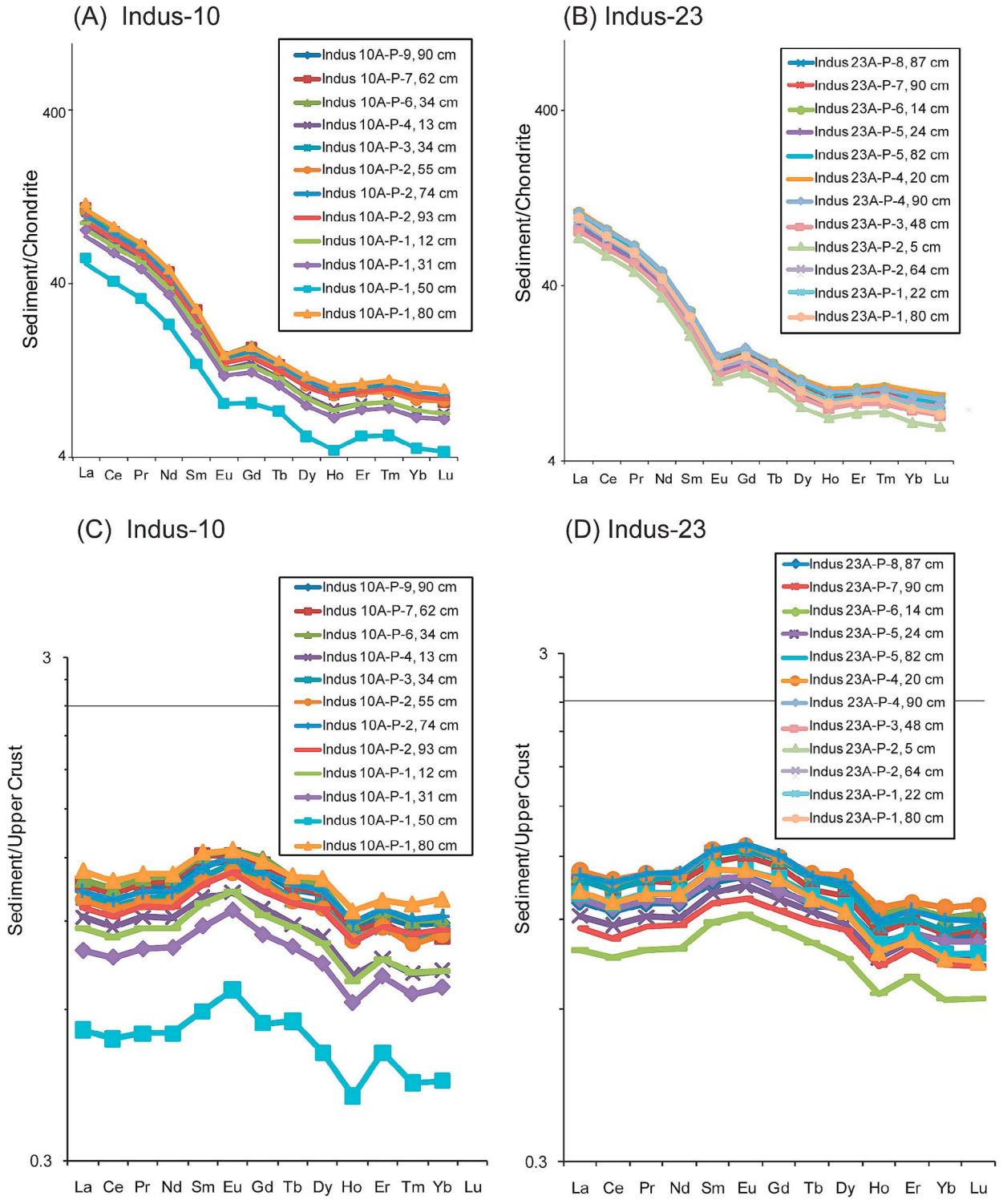

Figure 5. Rare earth element geochemistry normalized against chondrite [*Anders and Grevesse*, 1989] for (a) Site Indus-10 and (b) Site Indus-23 showing consistently high values for REEs at Site Indus-23 and much less variability compared to the sediment at Site Indus-10. (c) Normalized values against upper continental crust for Indus-10. (d) Normalized values against upper continental crust for Indus-23. Crust values from *Rudnick and Fountain* [1995].

correlate with the upper rise in ε_{Nd} values at 319 cm depth.

[23] In the latest Pleistocene to Early Holocene variability in sediment sources to site Indus-10 is evident in the ε_{Nd} values that vary between ca. −12 and −5. After 8 ka, with the exception of one sample, the ε_{Nd} values at Indus-10 are remarkably constant around −12 suggesting that sediments reaching the site come predominantly from a single, well-mixed source with sporadic sedimentary events originating from a secondary more primitive source. Similarly, at Indus-23 the ε_{Nd} values recorded at centennial scale for the last 1600 years suggest one predominant source of sediment with values between ca. −12 and −10 with subordinate influx from a secondary more primitive source. $^{87}Sr/^{86}Sr$ values are generally higher at Indus-23 compared to Indus-10, but this is because most of the Indus-23 samples are younger than 1.6 ka. When samples with the same age are compared then the values are close to one another. The $^{87}Sr/^{86}Sr$ value of the sediment beneath the unconformity at Indus-10 is close to the maximum values measured in Indus-23, but for much of the Holocene the $^{87}Sr/^{86}Sr$ values at Indus-10 are lower than seen more recently or under the Indus-10 unconformity. In both cores samples associated with higher ε_{Nd} values are slightly more depleted in REE concentrations.

6. Discussion

6.1. Significance of Geochemical Data

[24] Different elements display different degrees of mobility in aqueous fluids, so that during chemical weathering the ratios of water-mobile versus water-immobile elements change [*Nesbitt et al.*, 1980]. Alkali earth elements are commonly used in such proxies because they are relatively mobile and when compared to immobile elements track the degree of leaching (e.g., K/Al or K/Rb). K/Al may also reflect changing terrigenous supply or clay mineral input. It has been shown that K/Al relates to breakdown of K-feldspars and micas, as well as illite formation, which is associated with physical weathering of low grade metamorphic rocks [*Clift et al.*, 2008b].

[25] Mafic minerals are also generally less stable in continental environments than silica-rich minerals leading to their preferential breakdown and a loss of Mg in highly weathered rocks [*Lee et al.*, 2008]. This behavior lends itself to chemical weathering studies. Mg/Al has an advantage in showing no significant correlation with terrigenous mass accumulation rates, or with mean grain-size in a variety of settings [*Duzgoren-Aydin et al.*, 2002; *Price and Velbel*, 2003; *Schroeder and West*, 2005]. However, changes in carbonate content, especially dolomite will have a first order control on the Mg/Al ratios given the much higher mobility of carbonate bound Mg compared to silicate bound Mg. Mg/Al may thus at least partially track carbonate weathering. Because there is a significant amount of detrital carbonate present in the sediments exported by the Indus [*Garzanti et al.*, 2005] this influence must be assessed before the proxy can be simply interpreted.

[26] The chemical index of alteration (CIA) of *Nesbitt and Young* [1982] is a well-established weathering proxy. This is based on the relative mobility of Na, K and Ca in water relative to Al, which normally concentrates in the weathered rock. The CIA values were calculated using the method of *Nesbitt and Young* [1982] shown below.

$$CIA = [Al_2O_3/(Al_2O_3+CaO^*+Na_2O+K_2O] \times 100$$

CIA values are normally corrected for biogenic calcium, however where this data is unavailable the CaO^*/Na_2O ratio can be used instead of CaO* to yield a good estimate of CIA [*Singh et al.*, 2005]. The proximal location of the cores considered here means that the amount of pelagic biogenic material in these sediments is very low. However, the CIA does not correct for the presence of detrital carbonate grains and may be compromised as an effective proxy in this setting.

[27] We assess possible detrital carbonate control over our proposed weathering proxies by plotting each of them relative to CaO content and against Ti/Ca, which can be used as a proxy for clastic versus carbonate flux, including biogenic contents. Figures 6a–6d show that CIA and Mg/Al are closely correlated to the carbonate contents, so that more carbonate content gives the impression of less chemical weathering. K/Rb shows a different response but there is still a detectable correlation between this ratio and both CaO content and Ti/Ca (Figure 6e and 6f). K/Al seems to be the least affected of any of these proxies and shows no coherent link with either CaO or Ti/Ca.

[28] Application of the weathering proxies may also be affected by variations in grain size because finer grained material, especially clays tends to be more heavily weathered than sandier material. The cores are dominated by muddy, silty material outside a few sandy intervals and do not show major coherent

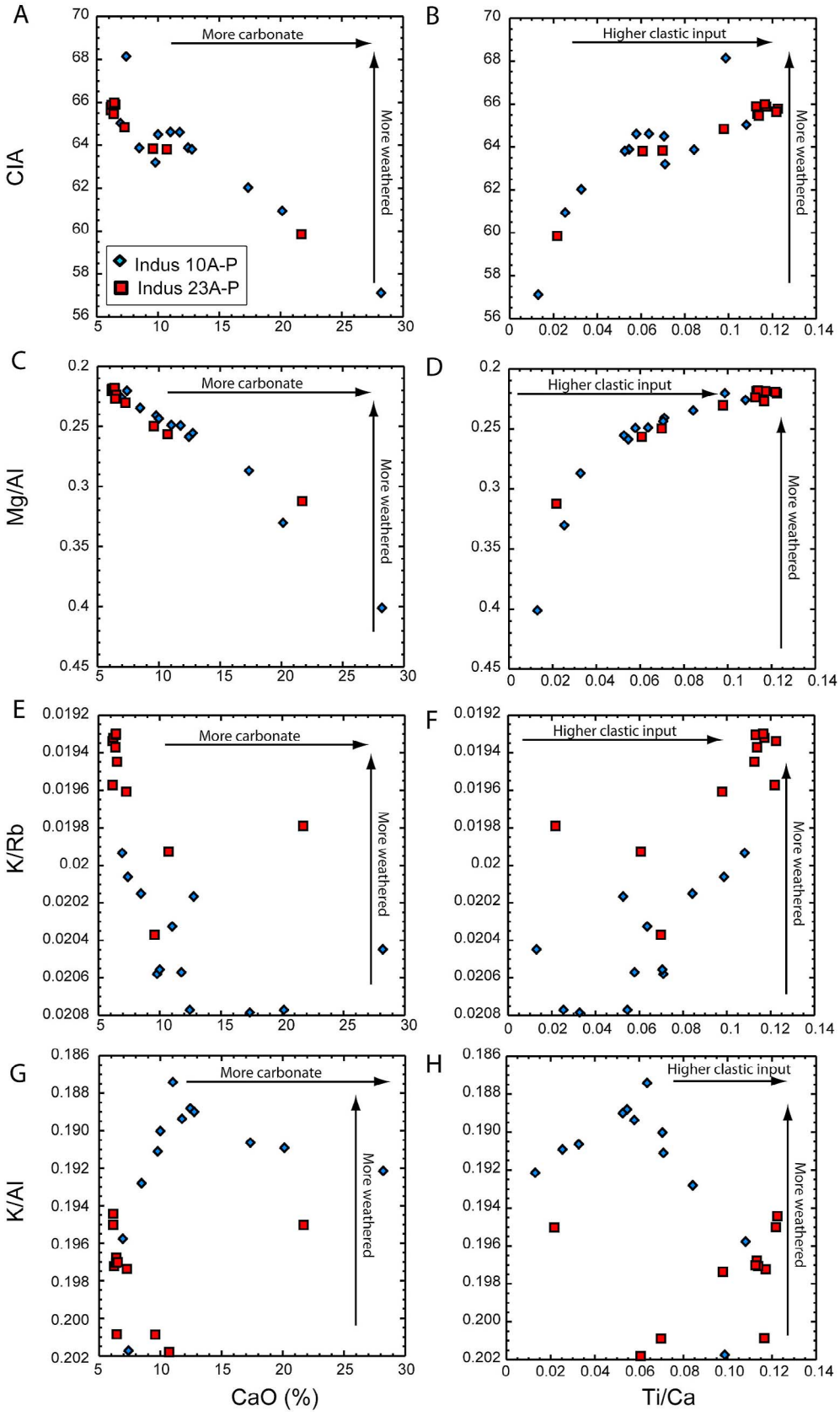
A
B
C
D
E
F
G
H
CIA
Mg/Al
K/Rb
K/Al
CaO (%)
Ti/Ca
More carbonate
Higher clastic input
More weathered
Indus 10A-P
Indus 23A-P

Figure 6

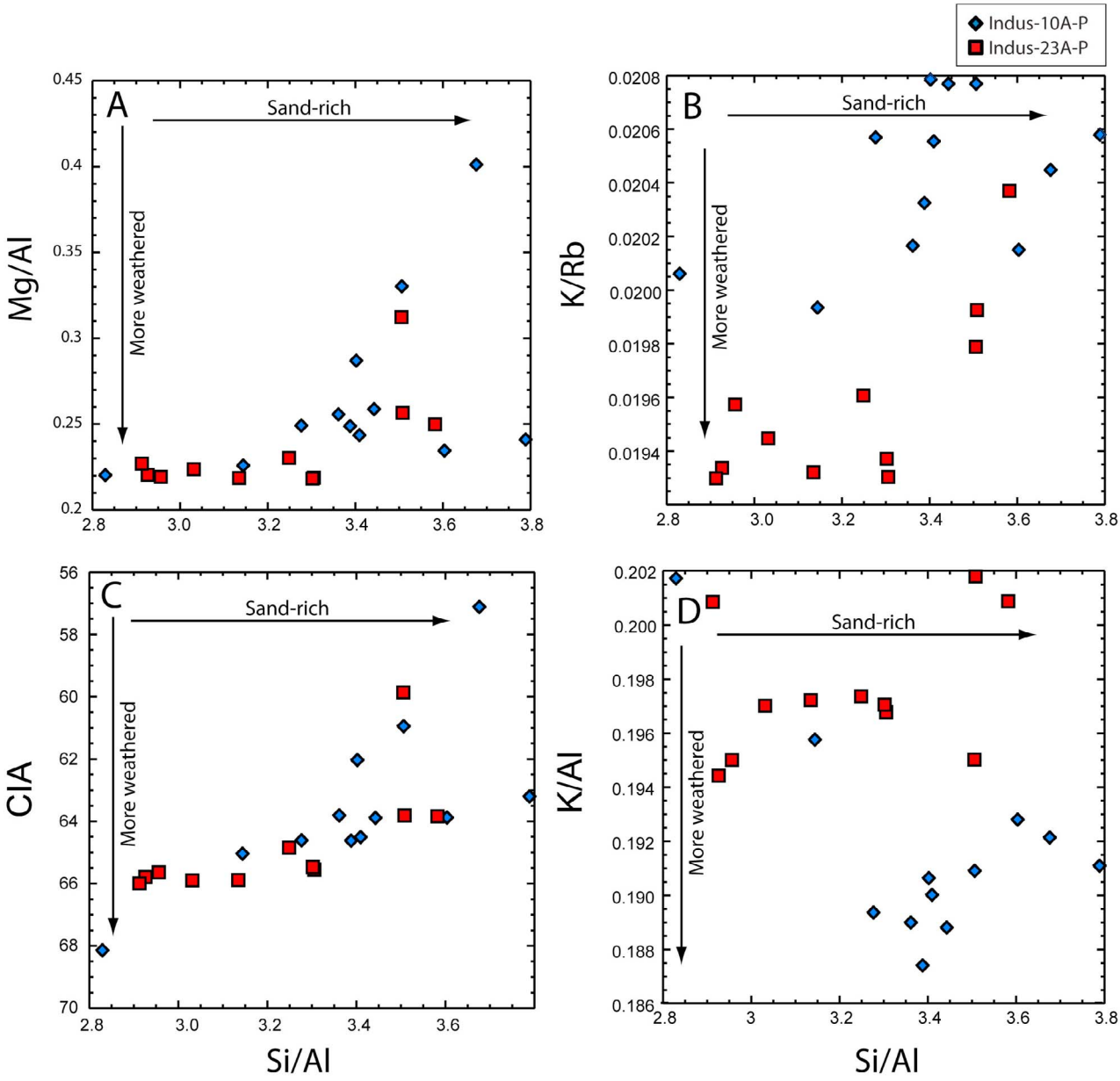

Figure 7. Crossplots showing various elemental ratios used for tracking chemical weathering intensity compared to Si/Al, considered a proxy for the proportion of sand and silt in the sediment.

departures in the average grain size up-section (Figures 3 and 4). Unfortunately the grain size data do not coincide with the geochemical analyses and so we test the links with grain size using Si/Al as a proxy based on the fact that Al is rich in clays, while Si is common in sands and silts as quartz grains. Figure 7 shows that many of the proxies are sensitive to this variability. Mg/Al is flat for the lowest Si/Al values but then rapidly increases. Again it is K/Al that appears to be uncorrelated with grain size, suggesting that it should make the most robust silicate weathering proxy.

Figure 6. Crossplots showing possible linked between various elemental ratios used for tracking chemical weathering intensity and the content of detrital carbonate in the sediment, as represented by CaO content and Ti/Ca. (a and b) For CIA, (c and d) for Mg/Al, (e and f) for K/Rb, and (g and h) for K/Al. Only K/Al shows no coherent link with Ca contents.

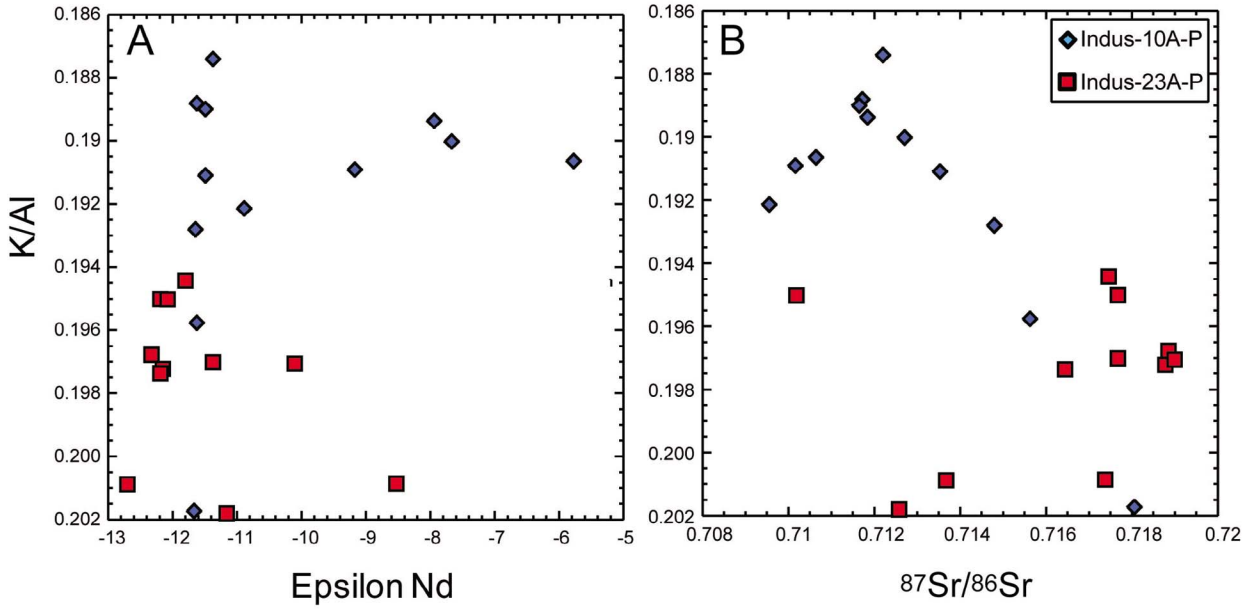

Figure 8. Variations in K/Al, considered a silicate weathering proxy and (a) Nd isotope character and (b) Sr isotope composition. Lower K/Al indicates more weathering and correlates with lower $^{7}Sr/^{86}Sr$ values.

[29] Sr and Nd isotopes have been used to track both provenance and weathering intensity. Sr isotopes fractionate $^{87}Sr/^{86}Sr$ values under the influence of chemical weathering, but can also be influenced by source composition, especially carbonate weathering [*Palmer and Edmond*, 1992]. Nd is largely unaffected by weathering and is a robust provenance proxy with wide earlier applications, including the Indus system [*Clift et al.*, 2002; *Clift and Blusztajn*, 2005]. Crucially Nd is not present in carbonate. Links have been made between Nd isotope character and grain size in eolian sediments [*Feng et al.*, 2009], although in marine sediments the link is less pronounced and is better displayed in terms of Sr [*Meyer et al.*, 2011]. Our data confirm this in showing a close link between $^{87}Sr/^{86}Sr$ values and CaO and no relationship with ε_{Nd} values. When we compare these isotopes to K/Al we see no link between K/Al and ε_{Nd} values, as might be expected (Figure 8). $^{87}Sr/^{86}Sr$ values do show a negative correlation with K/Al indicating that lower $^{87}Sr/^{86}Sr$ values are linked to more intense chemical weathering of silicates.

6.2. Temporal Variability

[30] The geochemical ratios shown in Figures 3 and 4 may be plotted against age calculated by assuming linear sedimentation rates between dated material (Figures 9a–9f and 10a–10f). The bottom of the core from Indus-23 is constrained as being 13.7 ka, based on the depth below modern sealevel and the anticipated age of post-glacial transgression [*Bard et al.*, 1996], as well as the ^{14}C ages. Figure 9a shows temporal variations in Mg/Al with a net decrease at Indus-10 from 0.5 to 0.25 since 11 ka, but with most of that change being between 11 ka and 8 ka. This may be interpreted as indicating decreasing carbonate weathering intensity at this time. Although there are not enough samples to estimate the trend during the Holocene at Indus-23, the centennial variability in Mg/Al over the last 1600 years is minimal with all samples except one at 0.25 similar to the corresponding sample at 0.8 ka from Indus-10 (Figure 10a). The sample at ca. 0.8 ka at Indus-10 is within the same range of Mg/Al variability as samples from Indus-23 over the last 1600 years.

[31] K/Rb is also interpreted as a chemical weathering proxy and this shows an increase in values (i.e., less intensity weathering or more carbonate flux) above the unconformity at Indus-10 compared to below. This could also suggest a loss of micas and feldspars though none are observed in microscopic analysis. Similar to Mg/Al, K/Rb falls from ~12 ka to the present-day, which could indicate increasing chemical weathering above the unconformity to the present-day or decreasing carbonate flux (Figure 7b). This similarity holds true for the CIA parameter as well (Figure 9d). The K/Rb

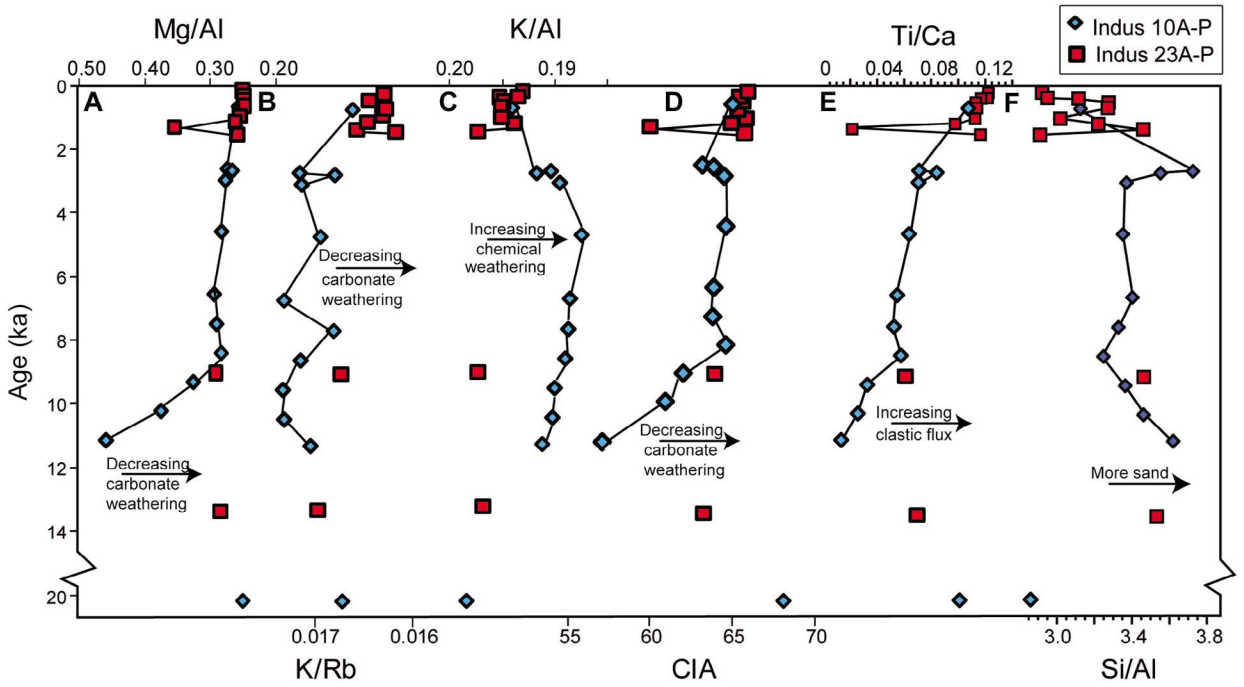

Figure 9. Temporal variations in geochemical ratios (a) Mg/Al, (b) K/Rb, (c) K/Al, (d) Chemical Index of Alteration (CIA), (e) Ti/Ca, and (f) Si/Al for Sites Indus-10 and -23 [*Nesbitt and Young*, 1982].

values at ca. 8.8 ka are slightly different at the two sites but care should be employed in interpreting this as a difference in weathering characteristics because the Early Holocene sedimentation at both sites is condensed and samples may not be coeval. In the last 1600 years (Figure 10b) changes in K/Rb closely match those of Mg/Al, although K/Rb shows a gradual fall that was not observed in the Mg/Al.

[32] K/Al is our most trusted proxy for chemical weathering of silicates and at Indus-10 there is a net decrease between 11 ka and 4 ka, indicating stronger chemical weathering, in agreement with Mg/Al (Figure 9c). The sample from below the unconformity has a high K/Al value despite the appearance in the core and the other weathering proxies indicating that it is strongly weathered prior to the postglacial transgression. After 4 ka K/Al increased to the present-day suggestive of less chemical weathering at 0–4 ka (Figure 9c) at odds with the Mg/Al trend. Indus-23 (Figure 10c) shows remarkably constant K/Al values in the last 1600 years. Similar K/Al values between 0.197 and 0.194 occur early during the Holocene at Indus-23. The Indus-23 sample at ca. 8.8 ka suggests less weathering at that time compared to at Indus-10, which contrasts with the CIA and Mg/Al indicating minor differences.

[33] Following very high CIA values under the LGM unconformity at Indus-10 CIA values fell at the time of transgression and then increased sharply between 11 ka and 8 ka, after which CIA is more constant (Figure 9d) suggesting stable weathering and provenance. At Indus-23 CIA values are consistent with the most recent Indus-10 samples, except for the low value sample at ca. 1.3 ka that was also anomalous in Mg/Al and K/Al values (Figure 10d).

6.3. Provenance

[34] Both sites have been influenced by the Southwest Monsoon and the westerlies, but potentially receive material from contrasting source regions. Indus-23 is presumed to receive sediment from the Indus River mouth, while Indus-10 could also receive influx from rivers in southwest Pakistan. Although longshore surface currents today are dominantly northward from Cape Monze during the summer (Figure 1) [*Elahi and Rashid*, 1981; *Schott and McCreary*, 2001] this may not have been the case when sea level was lower because the monsoonal conditions were different to the present-day causing shifts in the strength, direction and seasonality of the winds [*Clemens and Prell*, 1990] with consequences for coastal currents. Furthermore, a

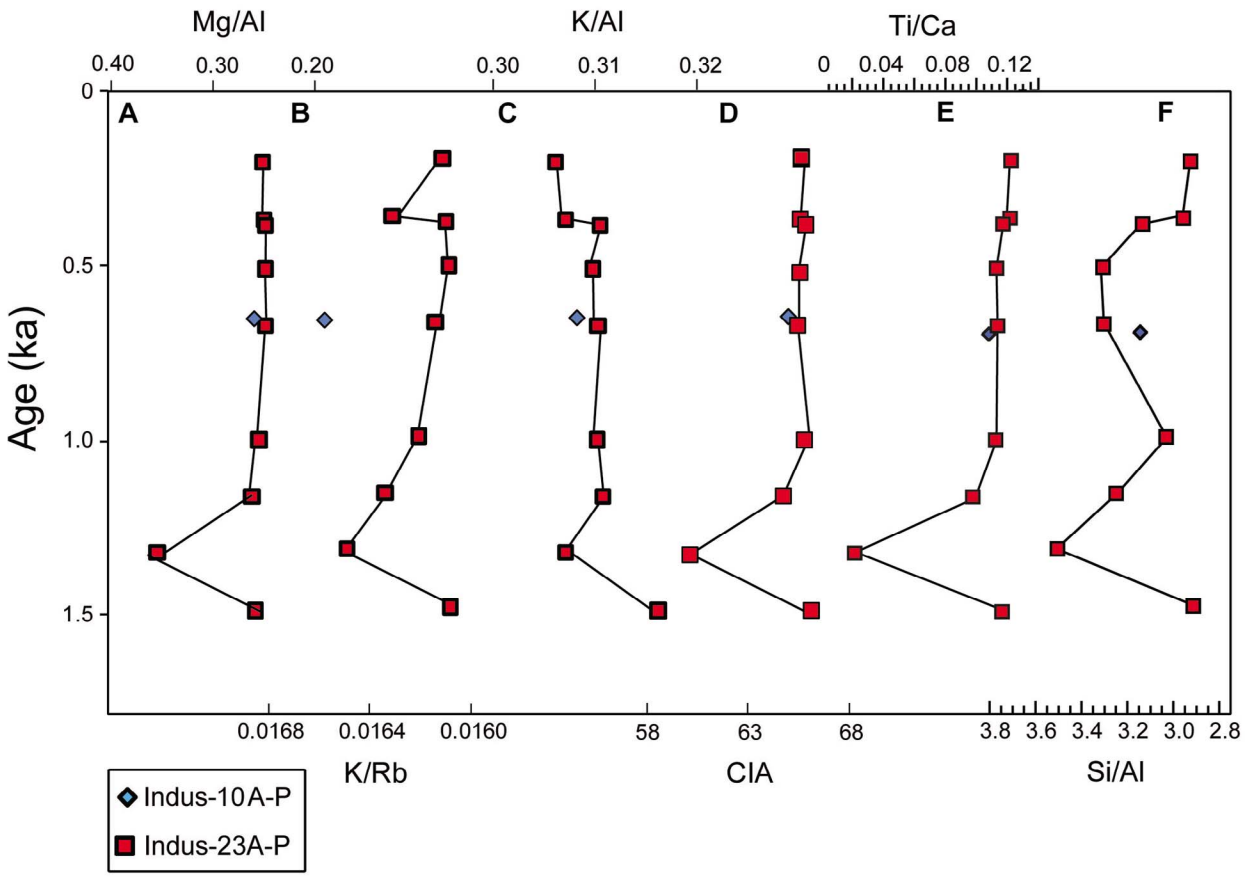

Figure 10. Temporal variations in geochemical ratios (a) Mg/Al, (b) K/Rb, (c) K/Al, (d) Chemical Index of Alteration (CIA), (e) Ti/Ca, and (f) Si/Al for Sites Indus-10 and -23 over the last 2,000 years.

rise in sea level would be necessary in order to develop the longshore current we see today. The base of Indus-10 is believed to be Pre-Holocene, given that the age of the unconformity is older than 10 ka, while the red-orange color of the sediment could suggest exposure to the surface. (Figures 2a and 3) Exposed shelf sedimentary deposits at the seafloor, especially on the outer shelf and close to the Murray Ridge (Figure 1) also provide possible sources of sediment during reworking in a high energy, wave dominated delta, such as the Indus. Comparison of provenance records from the two marine sites with the onshore record at Keti Bandar should constrain the fate of sediment reaching the Arabian Sea and the degree of reworking during Holocene sea level rise.

[35] The Indus Shelf does not necessarily record provenance changes seen in the Indus delta because of mixing with sediments from other sources and reworking of older shelf deposits. Here we explore this possibility using isotope data. Figure 11 compares temporal variations in ε_{Nd} and $^{87}Sr/^{86}Sr$ values for both core sites with the river mouth record at Keti Bandar [*Clift et al.*, 2010] in order to assess the whether the Indus Shelf can also record changes in Himalayan erosion. Most of the ε_{Nd} values from Sites Indus-10 and -23 lie within the range of previously published values for Indus Canyon sediments [*Clift et al.*, 2008a], but are typically shifted to slightly higher values compared to the synchronous values at the river mouth. ε_{Nd} values of −12 are recorded for much of the Holocene at Indus-10, which match analyses from suspended clay-rich sediment from the modern Indus River [*Goldstein et al.*, 1984]. These values are themselves higher than those derived from coarser-grained modern Indus river sediment [*Clift et al.*, 2002], and from finer grained Late Holocene sediment from Keti Bandar. This raises the possibility of a grain size control on Nd isotope character. However, within our data set there is no correlation between ε_{Nd}

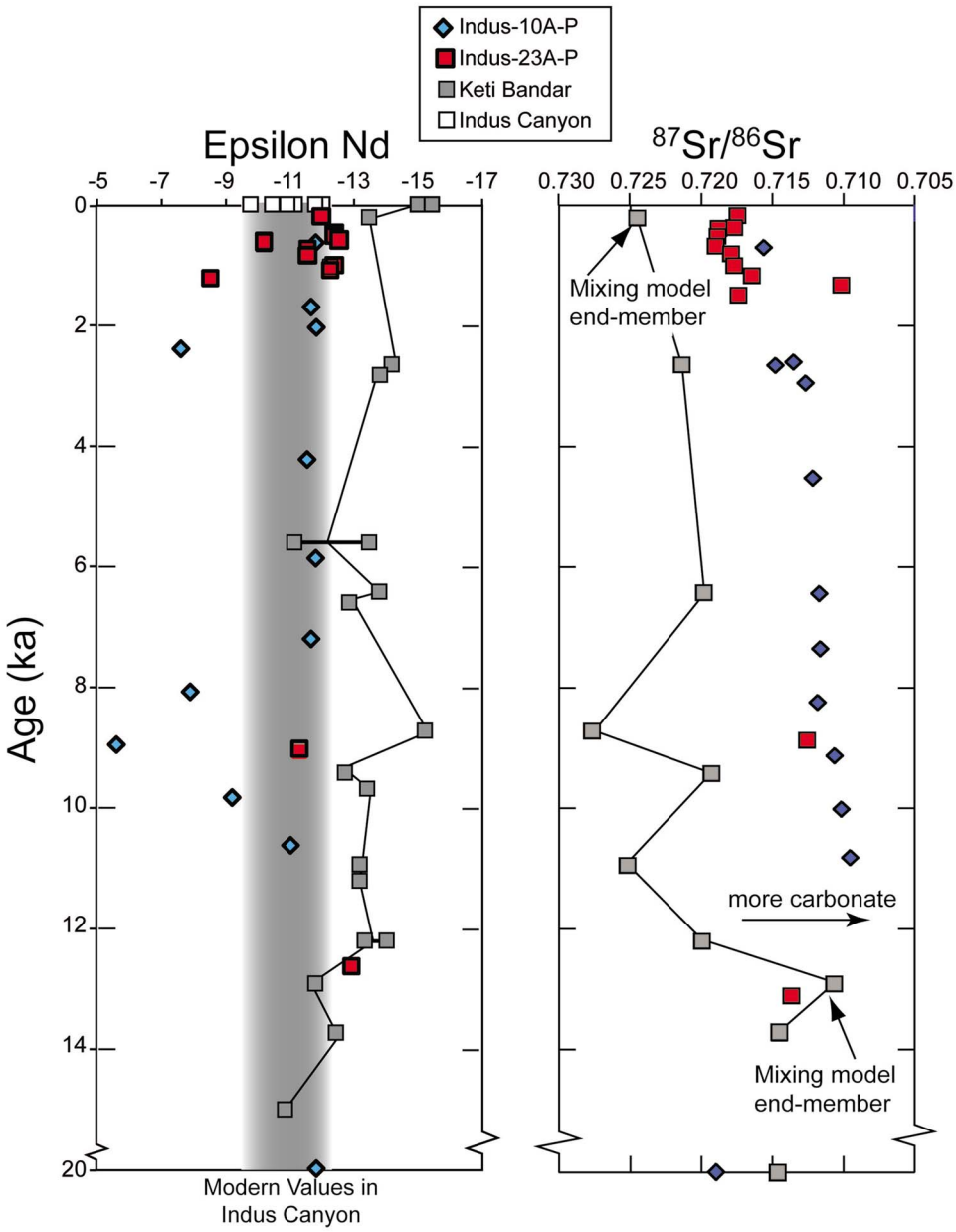

Figure 11. Comparison of the temporal evolution in onshore and offshore records of Nd and Sr isotopes through time in the Indus Delta since 20 ka. Keti Bandar data from *Clift et al.* [2008a, 2010]. Note the major differences in ε_{Nd} values between the marine cores and that taken at the coast at Keti Bandar, especially at 11–8 ka. Samples joined by horizontal line represent repeat analyses of material originally analyzed by *Clift et al.* [2008a].

values and Si/Al. $^{87}Sr/^{86}Sr$ values are affected by clay content, being higher with more clay (Figure 12c).

[36] The Lower Holocene (8–11 ka) from Indus-10 yielded three samples with ε_{Nd} values too high to have been derived only from the Indus River. A fourth sample dated at 2.95 ka also showed a high value. At Indus-23, where the record is mostly limited to the last 1600 years, the 1.3 ka sample also shows a contribution from a secondary source beyond the Indus River. Although ε_{Nd} values of between −4 and −8 have been recorded in the Indus River in such regions as the Karakoram and the Lhasa Block, these are at least ca. 1,000 km away from the shelf region and are mixed with more sediments of a more negative ε_{Nd} signature on their transport to the coast [*Clift et al.*, 2002]. In contrast to the ε_{Nd} values measured in Lower Holocene sediments at Indus-10 those of the same age at Keti

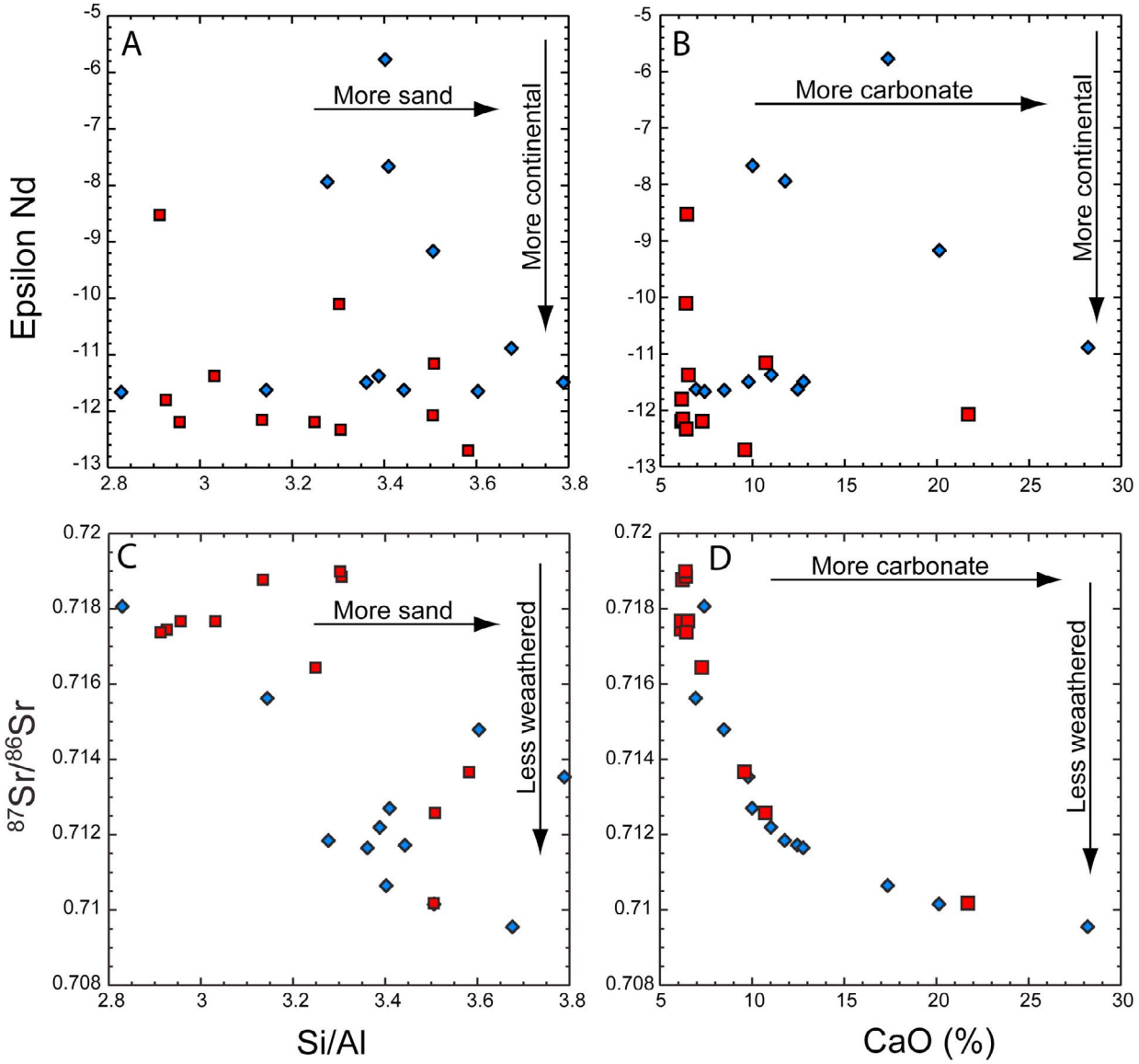

Figure 12. Plots showing links between Sr isotope character and (c, d) both carbonate content and grainsize, whereas (a, b) Nd isotopes do not correlate with either variable.

Bandar are much more negative, indicating influence of non-Indus source at Indus-10 at 8–11 ka.

[37] Since 7 ka there are differences between onshore and offshore cores records. The ε_{Nd} values for the most samples from the marine record above 7 ka are consistent with modern Indus Canyon samples rather than recent river sediments or the younger sediments at Keti Bandar. However, these sediments do correspond to Indus Delta sediments deposited before 13.5 ka [*Clift et al.*, 2008a], as well as the suspended sediment sample of *Goldstein et al.* [1984]. An offset between Keti Bandar and the marine cores is especially seen in $^{87}Sr/^{86}Sr$ for the Holocene, although the two sets do overlap at 13–15 ka. $^{87}Sr/^{86}Sr$ values are routinely lower on the shelf than at Keti Bandar. This is unlikely to be caused by grain size differences, as this influence would predict the opposite effect on $^{87}Sr/^{86}Sr$ values (Figure 12c). Shelf cores are typically finer than the river mouth and finer grain size are associated with higher $^{87}Sr/^{86}Sr$ values both here and in west Africa [*Meyer et al.*, 2011]. Because our shelf cores show lower $^{87}Sr/^{86}Sr$ values compared to the river this is probably not linked to grain size sorting. Rather the differences reflect a higher carbonate content in the shelf cores of both biogenic and detrital origin.

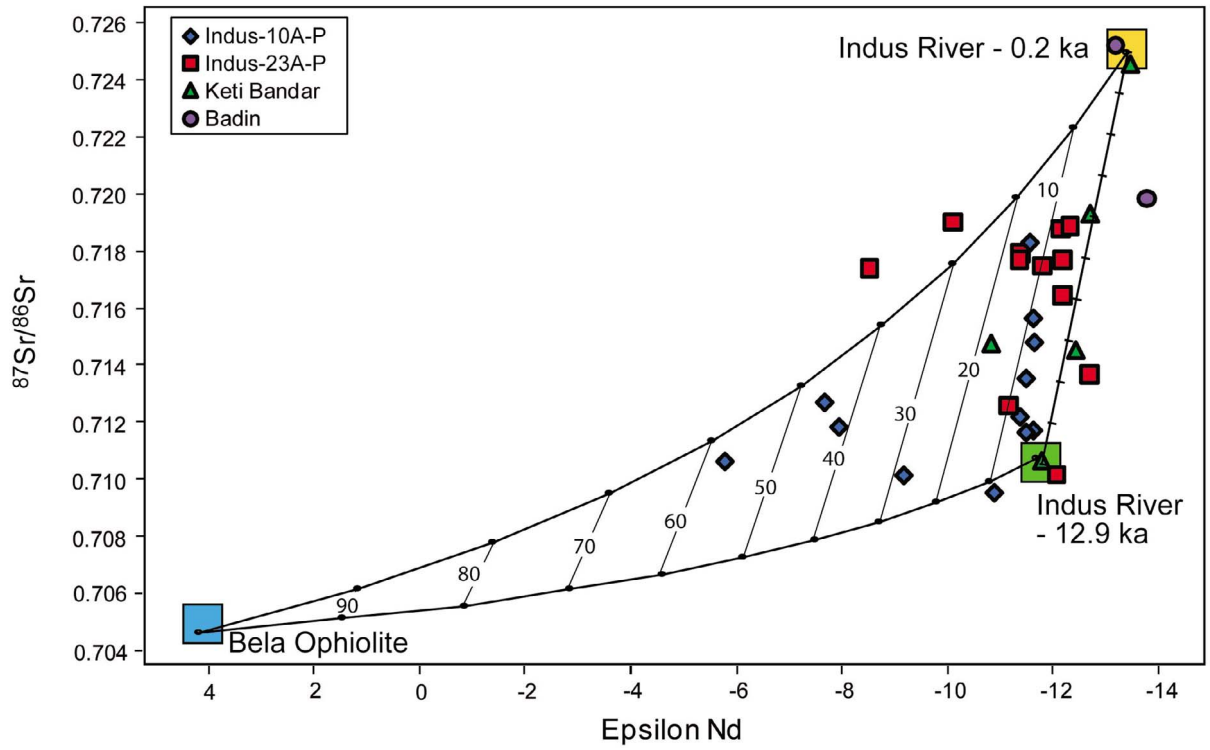

Figure 13. Relationship between strontium and neodymium isotopes for both onshore and offshore samples (latter data from *Clift et al.* [2008a] and data from the Bela Ophiolite [*Ahmed and Ernst*, 1999]). This clearly shows the marine samples plot between Indus River and Bela Ophiolite end-members. While the ophiolite is fixed in composition the Indus River end-members change through time. Mixing lines show 10% increments.

[38] The samples with particularly high ε_{Nd} values require explanation, as this difference cannot be due to differences in weathering histories. The REE character of the pre-7 ka samples from Indus-10 is more primitive and less continental then the younger samples. In order to yield ε_{Nd} values of between −4 and −7 a significant fraction of material with more positive values needs to be included in the bulk chemistry, together with the sediment sourced from the Indus. A candidate for the source of this material is the Bela Ophiolite, which formed during the Paleocene [*Umar et al.*, 2011] and is located in the Chaman fold thrust belt [*Zaigham and Mallik*, 2000], onshore and to the north of Indus-10. This area is drained by the Hab River [*Ahmed and Ernst*, 1999] (Figure 1), which enters the Arabian Sea approximately 20 km northwest of Karachi. ε_{Nd} values for the Bela Ophiolite range from between +4 and +7 [*Ahmed and Ernst*, 1999], well within what would be required to cause a shift to between −4 and −7. In contrast, the highest ε_{Nd} values known from the Indus River since the LGM are only −10.5 at Keti Bandar [*Clift et al.*, 2008a]. Figure 13 shows the relationship between Sr and Nd isotopes for our shelf samples, existing samples from the delta and the possible end-members. The Indus River is represented by two end-members because it changes its isotopic character significantly between the Last Glacial Maximum and the present-day [*Clift et al.*, 2010]. These end-members are defined by being the most isotopically extreme and these samples were dated as being 0.21 ka and 12.9 ka [*Clift et al.*, 2010]. The mixing calculations show that most of the samples lie between the Indus River end-members but that four samples from Indus-10 and two from Indus-23 have values that divert significantly from this array. The most extreme would imply >50% mixing of Indus River sediment with rock from the Bela Ophiolite. Even if that is an over-estimate it is clear that the isotopic range, especially on the western shelf, is greater than would be expected from a purely Indus source.

[39] If sediment flux from the Bela Ophiolite is the cause of the Nd isotope anomalies then the question remains of how this sediment was delivered to the core sites without being hugely diluted by the Indus River. There is a strong northwest to southeast longshore surface currents active during the Summer Monsoon [*Schott and McCreary*, 2001] and

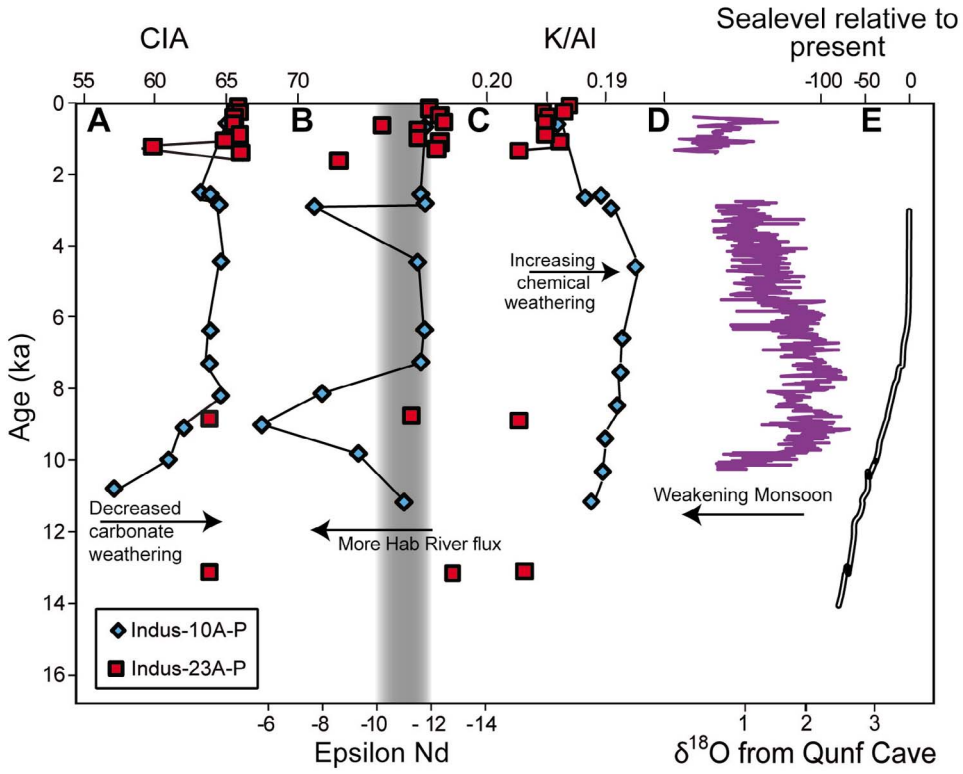

Figure 14. Selected proxies from our current data set against published records of climate and sea level change, (a) Chemical Index of Alteration, (b) Neodymium Isotopes, (c) K/Al, (d) Qunf Cave oxygen isotope record [*Fleitmann et al.*, 2003], and (e) sea level curve [*Bard et al.*, 1996].

modeling of currents along the Pakistani coast has shown that during the summer monsoon the dominant currents are from the northwest [*Elahi and Rashid*, 1981]. The low discharge of the Hab River compared to the Indus makes it very unlikely that suspended plumes of sediment could be bringing these sediments to the deeper parts of the shelf. However, assuming no subsidence, wave-driven longshore drift during the Early Holocene could be responsible for the Nd isotope anomalies at Indus-10 because at that time, when surf zone was deeper than present. Such a mechanism would have been terminated as sealevel rose and the coast migrated north.

[40] The isotopically and geochemically anomalous samples dated at 1.4 ka from Indus-23 and at 2.95 ka at Indus-10 are the only sediments that do not appear to be sourced solely from the Indus Delta since the Early Holocene. Because direct supply from the Hab River is not physically possible after 6 ka, we prefer to explain these anomalies as being caused by reworking of older shelf sediments. Seismic images of the shelf region ca. 10 km east and west of Indus-23, as well as close to Indus-10, show submerged outcrops but the composition of these rocks is unknown. However, outcrops of mid shelf deposits could contain sediments partly delivered alongshore from the Hab River during previous sea level cycles. It is possible that erosion of these outcrops is partly responsible for the occasional anomalously high ε_{Nd} values found in the Upper Holocene.

6.4. Climate and Weathering Records

[41] Comparing the various chemical proxies with established monsoon intensity records allows us to determine whether the monsoon is a primary control on weathering or provenance within the Indus Shelf. Figures 14a–14e plot the CIA, K/Al and Nd isotopic data against an oxygen isotope record from the Qunf Cave in southern Oman in which the oxygen isotope composition is linked to the intensity of summer rains [*Fleitmann et al.*, 2003]. The record indicates a strengthening summer monsoon between 11 ka and 8 ka.

[42] We have shown that CIA (as well as Mg/Al and $^{87}Sr/^{86}Sr$) values increased steeply at Indus-10

after 11 ka until 8 ka (Figure 14). This suggests that the strengthening of the monsoon during the Early Holocene had a major impact on reducing the flux of eroded carbonate in the sediments recovered at Indus-10. The Nd isotope data show a number of periods when the provenance was more influenced by the Hab River but these do not correlate either with monsoon history or with changes in CIA or K/Al. The silicate weathering tracked by K/Al shows a gradual increase in weathering between 11 ka and 4.5 ka, followed by a fall to the present-day. This history does not match the monsoon record. There is a 4–5 ka lag between peak monsoon strength and the peak in weathering intensity. This is even later than the peak chemical weathering identified from clay mineralogy at ca. 7 ka at Keti Bandar [*Alizai et al.*, 2012], and at ca. 6.5 ka on the Cochin-Kochi coast of western India [*Thamban et al.*, 2002]. However, in the case of our offshore record we cannot simply infer that this time lag represents the time needed for the weathering processes to respond to monsoon forcing because the combined isotope data indicate that the source of the sediment may be a mixture of newly delivered river sediments and reworked older deposits. While grain size sorting may have caused much of the isotopic differences seen between shelf and delta the data presented here does not presently favor this model, as we cannot demonstrate such a link in this system.

[43] Comparison of climate and ε_{Nd} values for Indus-10 (Figure 14) shows no clear control over provenance. However, we note that after 7 ka when sealevel is relatively stable ε_{Nd} values are generally constant, as might be expected for a well-mixed reservoir of sediments, such as wave-dominated shelf. Longshore transport from the Hab River to the area of Indus-10 was able to occur when the site was located near the coast, but by 8 ka sea level was only ca. 20 m lower than present levels [*Bard et al.*, 1996], thus cutting off the supply of isotopically primitive material from the west because Indus-10 was too deep to be exposed to longshore drift. Both sites have since been shielded from direct sediment flux from the NW by a bathymetric shoal extending off Cape Monze (Figure 1). Any shift in ε_{Nd} values after this time probably relates to reworking of sediment which may contain some Bela Ophiolite material deposited before the Holocene.

7. Conclusions

[44] Using geochemical analysis we have constrained the provenance of Holocene sediments that have accumulated on the Indus Shelf since 13 ka. The relatively high ε_{Nd} values and lower degrees of chemical weathering seen in Lower Holocene sediments at the western site Indus-10 indicate that a significant proportion of this sediment originated from the Bela Ophiolite via the Hab River along the coast to the northwest. Alternatively, the high ε_{Nd} signature may imply erosion of earlier deposits outcropping on the shelf, but which themselves received primitive material from the Bela Ophiolite. Other sedimentation is influenced by direct flux from the Indus River, as well as reworking of Indus shelf deposits. The isotopic differences between the shelf sediments at both sites and the delta may reflect a grain size sorting influence, although our data favor the presence of more carbonate offshore as the reason for the lower bulk $^{87}Sr/^{86}Sr$ values compared to the river mouth. Nonetheless, our sediments yield ε_{Nd} values that are consistently more positive than those seen at the river mouth and closer to values known from the LGM, suggesting that direct sediment supply from the river was not completely dominant. Sediment transport from the Hab River was possible during the Early Holocene because the transgression over a highly weathered basal Holocene unconformity placed Indus-10 temporarily close to the coast where it was able to receive sediment via the longshore drift. This flux was cut off as sea level continued to rise.

[45] Sediments at Indus-23 also have chemistries consistent with sediment supply from the Indus River mixed with some older Indus sediments. Similar to sediment from Indus-10, a sample dating from ca. 1.3 ka indicates a brief period of sediment flux from a secondary non-Indus source, probably reworked sediments from older shelf sequences. However, data from these buried outcrops needs to be obtained to establish an influence in sedimentary provenance. At Indus-10 an apparently sharp decrease in carbonate weathering flux between 11 ka and 8 ka may largely reflect the influx of poorly weathered material from the west mixing with detrital carbonate-bearing Indus River sediment at this time [*Staubwasser and Sirocko*, 2001]. K/Al appears to be the only chemical weathering proxy that is not affected by either grain size or carbonate content and this shows increasing weathering intensity from 11 to 4.5 ka, followed by a decrease the present-day. The trends in carbonate and silicate chemical weathering proxies do not readily correlate with the known variability of the SW summer monsoon, which strengthened from 11 ka to 8 ka and then weakened after 6 ka [*Fleitmann et al.*, 2003; *Gupta et al.*, 2003]. Consistent differences in Sr isotopic

values between the marine cores and sediments from the river mouth likely reflect more carbonate in the offshore, but the Nd isotope differences between shelf and delta imply that the direct flux from the river mouth is mixed with sediments reworked from pre-existing shelf deposits. Alternatively, we cannot exclude the idea that the composition of dominantly fine sediments on the shelf is affected by grain size sorting. Potential reworking or insufficient understanding of processes affecting proxies at their onland source highlight the complexity of interpreting fluvial and shelf sediments in terms of continental weathering and erosion records. By the same token, keeping in mind that shelf sediments feed the continental slope and the deep sea, this complexity is expected to translate to those environments as well.

Acknowledgments

[46] Cores were obtained on RV Pelagia cruise 64PE300 thanks to the professionalism of captain and crew, as well as the support staff at NIOZ and at National Oceanography Centre Southampton (NOCS). We thank NERC for funding this cruise and postcruise study. Award NSF-OCE 0623766 to LG also funded CP's participation to the cruise and postcruise studies. DL would also like to thank Guy Rothwell and Suzanne Maclachlan for permission to use BOSCORF facilities and Robyn Hannigan, Jeremy Williams, Tom Darrah and Sean McMahon for their discussion. Colin Taylor is thanked for assisting with the grain size analysis. PC thanks the Hanse Wissenschaftskolleg, Germany, for time to think about monsoonal river and delta systems. Two anonymous reviewers are also thanked for greatly improving the manuscript.

References

Ahmed, Z., and W. G. Ernst (1999), Island-arc related, back arc basinal and oceanic island complexes of the Bela Ophiolite-Mélange Complex, Pakistan, *Int. Geol. Rev.*, *41*, 739–763, doi:10.1080/00206819909465167.

Alizai, A., S. Hillier, P. D. Clift, and L. Giosan (2012), Clay mineral variations in Holocene terrestrial sediments from the Indus Basin: A response to SW Asian Monsoon variability, *Quat. Res.*, in press.

Anders, E., and N. Grevesse (1989), Abundances of the elements: Meteoric and solar, *Geochim. Cosmochim. Acta*, *53*, 197–214, doi:10.1016/0016-7037(89)90286-X.

Bard, E., B. Hamelin, M. Arnold, L. F. Montaggioni, G. Cabioch, G. Faure, and F. Rougerie (1996), Deglacial sea-level record from Tahiti corals and the timing of global meltwater discharge, *Nature*, *382*, 241–244, doi:10.1038/382241a0.

Bentahila, Y., O. Herbrard, D. B. Othman, J.-M. Luck, M. Serrane, and M. Lopez (2006), Gulf of Guinea Continental Slope and Congo (Zaire) deep sea fan: Sr-Pb isotopic constraints on sediment provenance from ZaiAngo cores, *Mar. Geol.*, *226*, 323–332, doi:10.1016/j.margeo.2005.11.014.

Böning, P., H.-J. Brumsack, B. Schnetger, and M. Grunwald (2009), Trace metal signatures of Chilean upwelling sediments at ~36°S, *Mar. Geol.*, *259*, 112–121, doi:10.1016/j.margeo.2009.01.004.

Burgess, P. M., and N. Hovius (1998), Rates of delta progradation during highstands: Consequences for timing of deposition in deep-marine systems, *J. Geol. Soc.*, *155*, 217–222, doi:10.1144/gsjgs.155.2.0217.

Clemens, S. C., and W. L. Prell (1990), Late Pleistocene variability of Arabian Sea summer monsoon winds and continental aridity: Eolian records from the lithogenic component of deep-sea sediments, *Paleoceanography*, *5*, 109–145, doi:10.1029/PA005i002p00109.

Clemens, S. C., D. W. Murray, and W. L. Prell (1996), Nonstationary phase of the Plio-Pleistocene Asian monsoon, *Science*, *274*, 943–948, doi:10.1126/science.274.5289.943.

Clift, P. D., and J. S. Blusztajn (2005), Reorganization of the western Himalayan river system after five million years ago, *Nature*, *438*, 1001–1003, doi:10.1038/nature04379.

Clift, P. D., et al. (2002), Nd and Pb isotope variability in the Indus River system; implications for sediment provenance and crustal heterogeneity in the western Himalaya, *Earth Planet. Sci. Lett.*, *200*, 91–106, doi:10.1016/S0012-821X(02)00620-9.

Clift, P., et al. (2008a), Holocene erosion of the Lesser Himalaya triggered by intensified summer monsoon, *Geology*, *36*, 79–82, doi:10.1130/G24315A.1.

Clift, P. D., K. Hodges, D. Heslop, R. Hannigan, L. V. Hoang, and G. Calves (2008b), Greater Himalayan exhumation triggered by Early Miocene monsoon intensification, *Nat. Geosci.*, *1*, 875–880, doi:10.1038/ngeo351.

Clift, P. D., et al. (2010), Monsoon control over erosion patterns in the Western Himalaya: Possible feed-backs into the tectonic evolution, in *Monsoon Evolution and Tectonics–Climate Linkage in Asia*, edited by P. D. Clift, R. Tada, and H. Zheng, *Geol. Soc. Spec. Publ.*, *342*, 185–218, doi:10.1144/SP342.12.

Colin, C., L. Turpin, J. Bertaux, A. Desprairies, and C. Kissel (1999), Erosional history of the Himalayan and Burman ranges during the last two glacial-interglacial cycles, *Earth Planet. Sci. Lett.*, *171*, 647–660, doi:10.1016/S0012-821X(99)00184-3.

Colin, C., G. Siani, M.-A. Sicre, and Z. Liu (2010), Impact of the East Asian monsoon rainfall changes on the erosion of the Mekong River basin over the past 25,000 yr, *Mar. Geol.*, *271*, 84–92, doi:10.1016/j.margeo.2010.01.013.

Derry, L. A., and C. France-Lanord (1996), Neogene Himalayan weathering history and river $^{87}Sr/^{86}Sr$; impact on the marine Sr record, *Earth Planet. Sci. Lett.*, *142*, 59–74, doi:10.1016/0012-821X(96)00091-X.

Dosseto, A., P. P. Hesse, K. Maher, K. Fryirs, and S. Turner (2010), Climatic and Vegetation control on sediment dynamics during the last glacial cycle, *Geology*, *38*, 395–398, doi:10.1130/G30708.1.

Duzgoren-Aydin, N. S., A. Aydin, and J. Malpas (2002), Re-assessment of chemical weathering indices: Case study of pyroclastic rocks of Hong Kong, *Eng. Geol. Amsterdam*, *63*, 99–119, doi:10.1016/S0013-7952(01)00073-4.

Elahi, K. Z., and K. Rashid (1981), A mathematical model of the northern Arabian Sea, *Ocean Manag.*, *6*, 149–158, doi:10.1016/0302-184X(81)90035-4.

Evrard, O., et al. (2010), Sediment dynamics during the rainy season in tropical highland catchments of central Mexico using fallout radionuclides, *Geomorphology*, *124*, 42–54, doi:10.1016/j.geomorph.2010.08.007.

Feng, J.-L., L.-P. Zhu, X.-L. Zhen, and Z.-G. Hu (2009), Grain size effect on Sr and Nd isotopic compositions in eolian dust:

Implications for tracing dust provenance and Nd model age, *Geochem. J.*, *43*, 123–131, doi:10.2343/geochemj.1.0007.
Fleitmann, D., S. J. Burns, M. Mudelsee, U. Neff, J. Kramers, A. Mangini, and A. Matter (2003), Holocene forcing of the Indian monsoon recorded in a stalagmite from southern Oman, *Science*, *300*, 1737–1739, doi:10.1126/science.1083130.
Garzanti, E., G. Vezzoli, S. Ando, P. Paparella, and P. D. Clift (2005), Petrology of Indus River sands: A key to interpret erosion history of the western Himalayan syntaxis, *Earth Planet. Sci. Lett.*, *229*, 287–302, doi:10.1016/j.epsl.2004.11.008.
Giosan, L., S. Constantinescu, P. D. Clift, A. R. Tabrez, M. Danish, and A. Inam (2006), Recent morphodynamics of the Indus delta shore and shelf, *Cont. Shelf Res.*, *26*, 1668–1684, doi:10.1016/j.csr.2006.05.009.
Goldstein, S. L., R. K. O'Nions, and P. J. Hamilton (1984), A Sm-Nd isotopic study of atmospheric dusts and particulates from major river systems, *Earth Planet. Sci. Lett.*, *70*, 221–236, doi:10.1016/0012-821X(84)90007-4.
Gupta, A. K., D. M. Anderson, and J. T. Overpeck (2003), Abrupt changes in the Asian southwest monsoon during the Holocene and their links to the North Atlantic Ocean, *Nature*, *421*, 354–357, doi:10.1038/nature01340.
Hughen, K. A., et al. (2009), Marine 04 radiocarbon calibration curves 0–50,000 years cal BP, *Radiocarbon*, *46*, 1059–1086.
Karim, A., and J. Veizer (2002), Water balance of the Indus river basin and moisture source in the Karakoram and western Himalayas: Implications from hydrogen and oxygen isotopes river water, *J. Geophys. Res.*, *107*(D18), 4362, doi:10.1029/2000JD000253.
Kessarkar, P. M., et al. (2005), Changing sedimentary environment during the Late Quaternary: Sedimentological and isotopic evidence from the distal Bengal Fan, *Deep Sea Res., Part I*, *52*, 1591–1615, doi:10.1016/j.dsr.2005.01.009.
Lee, C.-T. A., D. M. Morton, M. G. Little, R. Kistler, U. N. Horodyskyj, W. P. Leeman, and A. Agranier (2008), Regulating continent growth and composition by chemical weathering, *Proc. Nat. Acad. Sci.*, *105*, 4981–4986, doi:10.1073.pnas.0711143105.
McNichol, A. P., A. R. Gagnon, E. A. Osborne, D. L. Hutton, K. F. VonReden, and R. J. Schneider (1995), Improvements in procedural blanks at NOSAMS: Reflections of improvements in sample preparation and accelerator operation, *Radiocarbon*, *37*, 683–691.
Meyer, I., G. R. Davies, and J.-B. W. Stuut (2011), Grain size control on Sr-Nd isotope provenance studies and impact on paleoclimate reconstructions: An example from deep-sea sediments offshore NW Africa, *Geochem. Geophys. Geosyst.*, *12*, Q03005, doi:10.1029/2010GC003355.
Milliman, J. D., G. S. Quraishee, and M. A. A. Beg (1984), Sediment discharge from the Indus River to the Ocean: Past, Present and Future, in *Marine Geology and Oceanography of Arabian Sea and Coastal Pakistan*, edited by B. U. Haq and J. D. Milliman, pp. 65–84, Van Nostrand Reinhold, New York.
Nesbitt, H. W., and G. M. Young (1982), Early Proterozoic climates and plate motions inferred from major element chemistry of lutites, *Nature*, *299*, 715–717, doi:10.1038/299715a0.
Nesbitt, H. W., G. Markovics, and R. C. Price (1980), Chemical processes affecting alkalis and alkaline earths during continental weathering, *Geochim. Cosmochim. Acta*, *44*, 1659–1666, doi:10.1016/0016-7037(80)90218-5.
Palmer, M. R., and J. M. Edmond (1992), Controls over the strontium isotope composition of river water, *Geochim. Cosmochim. Acta*, *56*, 2099–2111, doi:10.1016/0016-7037(92)90332-D.
Price, J. R., and M. A. Velbel (2003), Chemical weathering indices applied to weathering profiles developed on heterogeneous felsic metamorphic parent rocks, *Chem. Geol.*, *202*, 397–416, doi:10.1016/j.chemgeo.2002.11.001.
Prins, M. A., G. Postma, J. Cleveringa, A. Cramp, and N. H. Kenyon (2000), Controls on terrigenous sediment supply to the Arabian Sea during the late Quaternary: The Indus Fan, *Mar. Geol.*, *169*, 327–349, doi:10.1016/S0025-3227(00)00086-4.
Prytulak, J., J. D. Vervoort, T. Plank, and C. Yu (2006), Astoria Fan sediments, DSDP site 174, Cascadia Basin: Hf-Nd-Pb constraints on provenance and outburst flooding, *Chem. Geol.*, *233*, 276–292, doi:10.1016/j.chemgeo.2006.03.009.
Rahaman, W., S. K. Singh, R. Sinha, and S. K. Tandon (2009), Climate control on erosion distribution over the Himalaya during the past ~100 ka, *Geology*, *37*, 559–562, doi:10.1130/G25425A.1.
Rudnick, R. L., and D. M. Fountain (1995), Nature and composition of the continental crust: A lower crustal perspective, *Rev. Geophys.*, *33*, 267–309, doi:10.1029/95RG01302.
Schattner, U., M. Lazar, G. Tibor, Z. Ben-Avraham, and Y. Makovsky (2010), Filling up the shelf- A sedimentary response to the last post glacial sea level rise, *Mar. Geol.*, *278*, 165–176, doi:10.1016/j.margeo.2010.10.006.
Schott, F. A., and J. McCreary (2001), The Monsoon circulation of the Indian Ocean, *Prog. Oceanogr.*, *51*, 1–23, doi:10.1016/S0079-6611(01)00083-0.
Schroeder, P. A., and L. T. West (2005), Weathering profiles developed on granitic mafic and ultramafic terrains in the area of Elberton, Georgia, *Ga. Geol. Soc. Guideb.*, *25*, 55–80.
Schulz, H., U. von Rad, and H. Erlenkeuser (1998), Correlation between Arabian Sea and Greenland climate oscillations of the past 110,000 years, *Nature*, *393*, 54–57.
Singh, M., M. Sharma, and H. J. Tobschall (2005), Weathering of the Ganga alluvial plain, northern India: Implications from fluvial geochemistry of the Gomati River, *Appl. Geochem.*, *20*, 1–21, doi:10.1016/j.apgeochem.2004.07.005.
Staubwasser, M., and F. Sirocko (2001), On the formation of laminated sediments on the continental margin off Pakistan; the effects of sediment provenance and sediment redistribution, *Mar. Geol.*, *172*, 43–56, doi:10.1016/S0025-3227(00)00119-5.
Thamban, M., V. P. Rao, and R. R. Schneider (2002), Reconstruction of late Quaternary monsoon oscillations based on clay mineral proxies using sediment cores from the western margin of India, *Mar. Geol.*, *186*, 527–539, doi:10.1016/S0025-3227(02)00268-2.
Tripathy, G. R., S. K. Singh, R. Bhushan, and V. Ramaswamy (2011), Sr–Nd isotope composition of the Bay of Bengal sediments: Impact of climate on erosion in the Himalaya, *Geochem. J.*, *45*, 175–186.
Umar, M., H. Friis, A. S. Khan, A. M. Kassi, and A. K. Kasi (2011), The effects of diagenesis on the reservoir characteristics in sandstones of the Late Cretaceous Pab Formation, Kirthar Fold Belt, southern Pakistan, *J. Asian Earth Sci.*, *40*, 622–635, doi:10.1016/j.jseaes.2010.10.014.
Vail, P. R., R. M. Mitchum, and S. Thompson (1977), Seismic stratigraphy and global changes of sea-level, in *Seismic Stratigraphy–Applications to Hydrocarbon Exploration*, edited by C. E. Payton, *AAPG Mem.*, 26, 63–81.
Valdiya, K. S. (1999), Rising Himalaya: Advent and intensification of monsoon, *Curr. Sci.*, *76*, 514–524.
von Rad, U., and M. Tahir (1997), Late Quaternary sedimentation on the outer Indus shelf and slope (Pakistan): Evidence from high-resolution seismic data and coring, *Mar. Geol.*, *138*, 193–236, doi:10.1016/S0025-3227(96)00090-4.

Wan, S., J. Tian, S. Steinke, A. Li, and T. Li (2010), Evolution and variability of the East Asian summer monsoon during the Pliocene: Evidence from clay mineral records of the South China Sea, *Palaeogeogr. Palaeoclimatol. Palaeoecol.*, *293*, 237–247, doi:10.1016/j.palaeo.2010.05.025.

Weber, M. E., M. H. Wiedicke, H. R. Kudrass, C. Hübsche, and H. Erlenkeuse (1997), Active growth of the Bengal Fan during sea-level rise and highstand, *Geology*, *25*, 315–318, doi:10.1130/0091-7613(1997)025<0315:AGOTBF>2.3.CO;2.

West, A. J., A. Galy, and M. J. Bickle (2005), Tectonic and climatic controls on silicate weathering, *Earth Planet. Sci. Lett.*, *235*, 211–228, doi:10.1016/j.epsl.2005.03.020.

Zaigham, N. A., and K. A. Mallik (2000), Bela ophiolite of southern Pakistan: Tectonic setting and associated mineral deposits, *Geol. Soc. Am. Bull.*, *112*, 478–489, doi:10.1130/0016-7606(2000)112<478:BOZOSP>2.0.CO;2.